Experimental evidence for Sulphide Magma Percolation and Evolution: relevant to the chromite bearing reefs of the Bushveld Complex

by

Corné Koegelenberg

Thesis presented in partial fulfillment of the requirements for the degree of

Masters in Geology at Faculty of Science, University of Stellenbosch

Supervisor: **Professor Gary Stevens**

Faculty of Science
Department of Earth Science

March 2012

***

Foreword

The entirety of my research work towards my MSc is contained within the paper that forms the basis of this thesis. The paper has been submitted to the Journal of Economic Geology and is currently under review (Prof. Gary Stevens as corresponding author). The paper has three authors and the role of each of these is as follows: Corne Koegelenberg. I am the lead author as I conducted the research and wrote the manuscript. All the experiments reported within the thesis are my own and these experiments were performed by my own hands. I prepared all run products for analysis and performed the analyses. The data processing and interpretation are my own work; Luhann Theron's MSc project ran in parallel with my own and we worked together on preparing the starting material which is shared by both our studies. Luhann's work focussed on phase relations in sulphide magna and partitioning of Pt between phases within the magma, at 1 atm. Luhann is a co-author because of his contribution to the development of the starting material and the understanding of phase relations in the sulphide system. His MSc similarly constitutes a manuscript that has been submitted to Economic Geology and I am 2nd author on that work; Gary Stevens contributed the research idea, provided guidance on experimental design, analytical techniques, data interpretation etc. He guided the writing of the thesis by commenting on numerous drafts of the manuscript.

Declaration

By submitting this thesis/dissertation electronically, I declare that the entirety of the work contained therein is my own, original work, that I am the sole author thereof (save to the extent explicitly otherwise stated), that reproduction and publication thereof by Stellenbosch University will not infringe any third party rights and that I have not previously in its entirety or in part submitted it for obtaining any qualification.

Signature: ……

Date: ……

Abstract

Pt mineralization within the Bushveld Complex is strikingly focused on the chromitite reefs, despite these horizons being associated with low volumes of base metal sulphide relative to Pt grade. Partitioning of Pt ($D_{sil/sulp}$) from silicate magma into immiscible sulphide liquid appears unable to explain Pt concentrations in chromitite horizons, due to the mismatch that exists between very large R factor required and the relevant silicate rock volume. Consequently, in this experimental study we attempt to gain better insight into possible Pt grade enhancement processes that may occur with the Bushveld Complex (BC) sulphide magma. We investigate the wetting properties of sulphide melt relevant to chromite and silicate minerals, as this is a key parameter controlling sulphide liquid percolation through the cumulate pile. Additionally, we have investigated how fractionation of the sulphide liquid from mono-sulphide-solid-solution (Mss) crystals formed within the overlying melanorite might affect sulphide composition and Pt grades within the evolved sulphide melt. Two sets of experiments were conducted: Firstly, at 1 atm to investigate the phase relations between 900^{O}C and 1150^{O}C, within Pt-bearing sulphide magma relevant to the BC; Secondly, at 4 kbar, between 900^{O}C to 1050^{O}C, which investigated the downwards percolation of sulphide magma through several layers of silicate (melanorite) and chromitite. In addition, 1atm experiments were conducted within a chromite dominated chromite-sulphide mixture to test if interaction with chromite affects the sulphide system by ether adding or removing Fe^{2+}. Primary observations are as follows: We found sulphide liquid to be extremely mobile, the median dihedral angles between sulphide melt and the minerals of chromitite and silicate layers are 11^{O} and 33^{O} respectively. This is far below the percolation threshold of 60^{O} for natural geological systems. In silicate layers sulphide liquid forms vertical melt networks promoting percolation. In contrast, the extremely effective wetting of sulphide liquid in chromitites restricts sulphide percolation. Inter-granular capillary forces increase melt retention, thus chromitites serve as a reservoir for sulphide melt. Sulphide liquid preferentially leaches Fe^{2+} from chromite, increasing the Fe concentration of the sulphide liquid. The reacted chromite rims are enriched in spinel end-member. This addition of Fe^{2+} to the sulphide magma prompts crystallization Fe-rich Mss, decreasing the S-content of sulphide melt. This lowers Pt solubility and leads to the formation of Pt alloys within the chromitite layer. Eventually, Cu-rich sulphide melt escapes through the bottom of the chromitite layer.

These observations appear directly applicable to the mineralized chromitite reefs of the Bushveld complex. We propose that sulphide magma, potentially injected from the mantle

with new silicate magma injections, percolated through the silicate cumulate overlying the chromitite and crystallized a significant volume of Fe-Mss. Chromitite layers functioned as traps for percolating, evolved, Cu-, Ni- and Pt-rich sulphide liquids. This is supported by the common phenomenon that chromitites contain higher percentages of Ni, Cu and Pt relative to hanging wall silicate layers. When in contact with chromite, sulphide melt is forced to crystallize Mss as it leaches Fe^{2+} from the chromite, thereby further lowering the S-content of the melt. This results in precipitation, as Pt alloys, of a large proportion of the Pt dissolved in the sulphide melt. In combination, these processes explain why chromitite reefs in the Bushveld Complex have Pt/S ratios are up to an order of magnitude higher that adjacent melanorite layers.

Opsomming

Pt mineralisasie in die Bosveld Kompleks is kenmerkend gefokus op die chromatiet riwwe, alhoewel die riwwe geassosieer is met lae volumes basismetaal sulfiedes relatief tot Pt graad. Verdeling van Pt ($D_{sil/sulp}$) vanaf silikaat magma in onmengbare sulfiedvloeistof is klaarblyklik onvoldoende om Pt konsentrasies in chromatiet lae te verduidelik, a.g.v. die wanverhouding wat bestaan tussen ‘n baie groot R-faktor wat benodig word en die relatiewe silikaat rots volumes. Gevolglik, in die eksperimentele studie probeer ons beter insig kry oor moontlike Pt graad verhogingsprosesse wat plaasvind in die BK sulfied magma. Ons ondersoek die benattingseienskappe van sulfied vloeistof relevant tot chromiet- en silikaat minerale, omdat dit die sleutel maatstaf is vir die beheer van sulfied vloeistof deursypeling deur die kumulaat opeenhoping. Addisioneel het ons ook ondersoek hoe die fraksionering van sulfied vloeistof vanaf MSS kristalle, gevorm binne die hangende melanoriet muur, moontlik die sulfied samestelling en Pt graad binne ontwikkelde sulfied smelt kan beïnvloed. Twee stelle van eksperimente is gedoen: Eerstens, by 1 atm om ondersoek in te stel oor fase verwantskappe tussen 900^{O}C en 1150^{O}C, binne ‘n Pt-verrykte sulfied magma samestelling relevant tot die BK; Tweedens, by 4 kbar, tussen 900^{O}C tot 1050^{O}C, wat die afwaartse deursypeling van sulfied magma deur veelvuldige lae van silikaat minerale en chromatiet. Addisionele 1 atm eksperimente is gedoen binne ‘n chromiet gedomineerde chromiet-sulfied mengsel, om te toets of interaksie met chromiet die sulfied sisteem affekteer deur Fe^{2+} te verwyder of by te dra. Primêre observasies is soos volg: Ons het bevind sulfiedsmelt is uiters mobiel, die mediaan dihedrale hoek tussen sulfiedsmelt en minerale van chromiet en silikaat lae is 11^{O} en 33^{O} onderskydelik. Dit is ver onder die deursypelings drumpel van 60^{O} vir natuurlike geologiese stelsels. In silikaatlae vorm die sulfiedsmelt vertikale netwerke wat deursypeling bevorder. Inteendeel, uiters effektiewe benatting van sulfiedsmelt binne chromatiete vertraag sulfied deusypeling. Tussen kristal kapilêre kragte verhoog smelt retensie, dus dien chromatiete as ‘n opgaarmedium vir sulfiedsmelt. S oorversadigte sulfied vloeistof loogsif Fe^{2+} vanuit chromiet en veroorsaak ‘n verhoging in Fe-konsentraie. Die gereageerde chromiet buiterante is daarvolgens verryk in Cr-spinêl eind-ledemaat. Die addisionele byvoeging van Fe^{2+} aan sulfied magma veroorsaak die kristalisasie van Fe-ryke Mss en verlaag dus die S-konsentrasie van die sulfied smelt. Dit verlaag Pt oplosbaarheid en lei tot die formasie van Py allooie binne-in chromatiete. Ten einde, ontsnap Cu-ryke sulfied smelt deur die onderkant van die chromatiet lae.

Die observasies is direk van toepassing op die gemineraliseerde chromatiet riwwe van die Bosveld Kompleks. Ons stel voor dat sulfied magma, potensiaal ingespuit vanuit die mantel saam nuwe inspuitings van silikaat magma, deur die hangende silikaat kumulaat bo chromatiet lae deurgesypel het en ‘n betekenisvolle volume Fe-Mss gekristalliseer het. Chromatiet lae het gefunksioneer as lokvalle vir afwaartsbewegende, ontwikkelde, Cu-, Ni-, en Pt-ryke sulfied vloeistowwe. Dit word ondersteun deur die algemene verskynsel dat chromatiete hoër persentasies van Ni, Cu en Pt relatief teenoor die hangende muur silikaat lae het. Wanneer sulfied smelt in kontak is met chromiet, word dit geforseer om Mss te kristalliseer soos Fe^{2+} geloogsif word, waarvolgens die smelt se S konsentrasie verder verlaag word. Dit veroorsaak die presipitasie, as Pt allooie, van groot proporsies opgeloste Pt vanuit sulfied smelt. Deur die prosesse te kombineer, kan dit moontlik verduidelik word hoekom chromatiet riwwe in die Bosveld Kompleks Pt/S verhoudings veel hoër is as aanrakende melanoriet lae.

Acknowledgements

An introduction into experimental petrology requires immense technical support and a daring, sometimes unconventional, approach to systematically constrain and solve peterological riddles. I cannot claim that the ideas are merely my own, but a product of continued collaboration between myself, Professor Gary Stevens and Luhann Theron. As my supervisor, Professor Gary Stevens, provided me with a platform to learn and develop as a scientist, creating an environment promoting good communication and collaboration with fellow students. My humble gratitude goes out to him for his continuous financial support and providing the necessary facilities to make this study possible. I'd like to thank my co-worker and friend, Luhann Theron, for his willing support through all the electric shocks, explosions, burns and seemingly endless maintenance problems. Thanks to the Chemical Engineering Department for lending us their vertical furnaces and facilities, Madelain Frasenburg for her guidance on the SEM, and Technical assistant George Olivier for organizing supplies.

Contents

1. General introduction 11
2. Presentation of Paper 14
    - Introduction 16
    - Geology of the Bushveld Complex 17
    - Sulphide melt as a collector of PGE 19
    - Extreme Pt/S in chromitites 19
    - Sulphide Melt Wetting 23
    - Experimental sulphide phase relations 23
    - Sulphide experiments 25
        - Sulphide composition 25
        - Synthesis of starting material 26
        - 1 Atm experiments 26
        - 4 Kbar experiments 27
        - Analytical methods 29
    - Results 29
        - 1 Atm sulphide phase relations 29
        - 4 Kbar textural analysis 32
        - Sulphide compositions 35
        - Chromite compositions 39
        - Dihedral angle measurements 41
    - Discussion 41
        - Sulphide melt mobility 41
        - Sulphide melt – chromite interaction 44
        - Crystallization of platinum alloys 45
    - Model for Bushveld Pt mineralization 46
    - Conclusion 48
    - References 49
3. Appendix 53

List of Figures

1.1 Geological map of the Bushveld Complex..... 12

Figures within Paper:

1 A schematic log section of the RLS, showing evolution of whole rock Sr^{87}/Sr^{86} initial isotopic ratios and lithology. 18

2 An illustration of a normal Merensky reef log section, showing PGE tenor, Pt/S and bulk rock Cu, Ni and S wt%, with respect to lihological stratigraphy..... 22

3 Sulphide phase relations in the 1atm Fe-Ni-S, Cu-Fe-S, and Cu-Ni-S ternary system with 0.4 - 0.5 wt% PGE added at $980^{O}C$-$1000^{O}C$ 25

4 gray scale X-ray maps of the quenched sulphide melt synthesised at $1200^{O}C$ and 1Atm. 27

5 19mm pressure cell design 28

6 1Atm textures 31

7 4Kbar textures 34

8 A BSD image and associated X-ray elemental maps of S, Fe, Ni and Cu illustrating typical compositional trends of sulphide at multiple temperatures at 4kbar. 37

9 Plots of compositional variation between starting chromite, re-crystallized chromite and chromite rims that has interacted with sulphide melt. 40

10 SEM BSD images of layered charge at 4Kbar, $1000^{O}C$ (24h)..... 43

11 Model for Pt mineralization 47

List of Tables

Tables within paper:

1. 1 Atm sulphide compositions 38

2. 4 Kbar sulphide compositions 38

3. Average chromite compositions 39

4. Dihedral angle measurements 41

1. General Introduction

The Bushveld Complex (BC) is the world's largest known layered mafic to ultramafic igneous intrusion. It extends 450km east-west and 350km north-south with a maximum thickness approaching 8km (figure 1.1). The continuity of individual lithological layers in the Bushveld is extraordinary with some traceable along strike for over 150km. It is primarily hosted within country rocks of the Transvaal Supergroup, however in the northern extreme Archean granitiods and greenstones form the footwall of the complex (Naldrett et al, 2009[b]). Apart from the geological significance, it also contains 95% of the worlds PGM (platinum group minerals) reserves (USGS mineral publications, PGM, 2010) making it arguably the most valuable ore body on earth. Despite the enormous size, PGE (platinum group elements) mineralization is strikingly focussed on the chromitite horizons of the sulphide rich Merensky and UG2 reefs located in the upper Critical Zone of the Rustenburg Layered Series (RLS) (figure1.1).

The mechanisms by which the association between chromitite and PGE concentration is achieved are not clear, however it is argued that sulphide melt had an important role to play considering that other PGE mineralized reefs in the Bushveld, e.g. Platreef, contain almost no chromite (Cawthorn, 1999). Current Bushveld Complex (BC) mineralization models struggle to address the details of the role played by the sulphide fraction of the magma. For example, if PGE's have been concentrated in chromitite by immiscible sulphide liquids, why are the PGE concentrations in the reefs apparently too high to be reconciled with their current sulphide contents (Godel et al, 2007)? The problem of low sulphide content in chromitite reefs has prompted several authors to suggest firstly, that some PGE has been concentrated by chromite itself during crystallization directly out of the silicate magma prior to sulphide saturation (e.g. Naldrett et al, 2009[a]); or secondly, that chromitite reefs lost sulphur due to the breakdown of interstitial sulphide via interaction with chromite minerals (Naldrett & Lehmann, 1988). These arguments continue despite limited experimental knowledge to how sulphide melt physically and chemically behaves in a layered silicate and chromite cumulate environment. Currently, natural rock studies suggest that chromitite may have acted as a barrier or filter, trapping dense percolating sulphide melt (Godel et al, 2006 & 2007), however the degree to which re-crystallised and annealed natural samples reflect the true sulphide melt silicate- and chromite-mineral interaction surfaces is uncertain. Sub solidus re-crystallization and re-equilibration of sulphide assemblages during cooling (Merke, 1992;

Coghill & Wilson, 1998) completely transforms original, high-temperature sulphide textures and phases.

The paper presented in this thesis adopts an experimental approach in order to investigate the physical and chemical properties of Pt enriched sulphides in a high temperature state (>900^{O}C), with a specific emphasis on layered chromitite bearing reefs (e.g. Merensky, UG-2). This will allow sulphide, chromite and silicate systems to be cooled rapidly minimizing the effects of re-equilibration and re-crystallization, hence preserving high temperature textures. Ultimately, we aim to increase the current understanding of how sulphides contribute to Pt mineralization, which will be useful in producing refined exploration models.

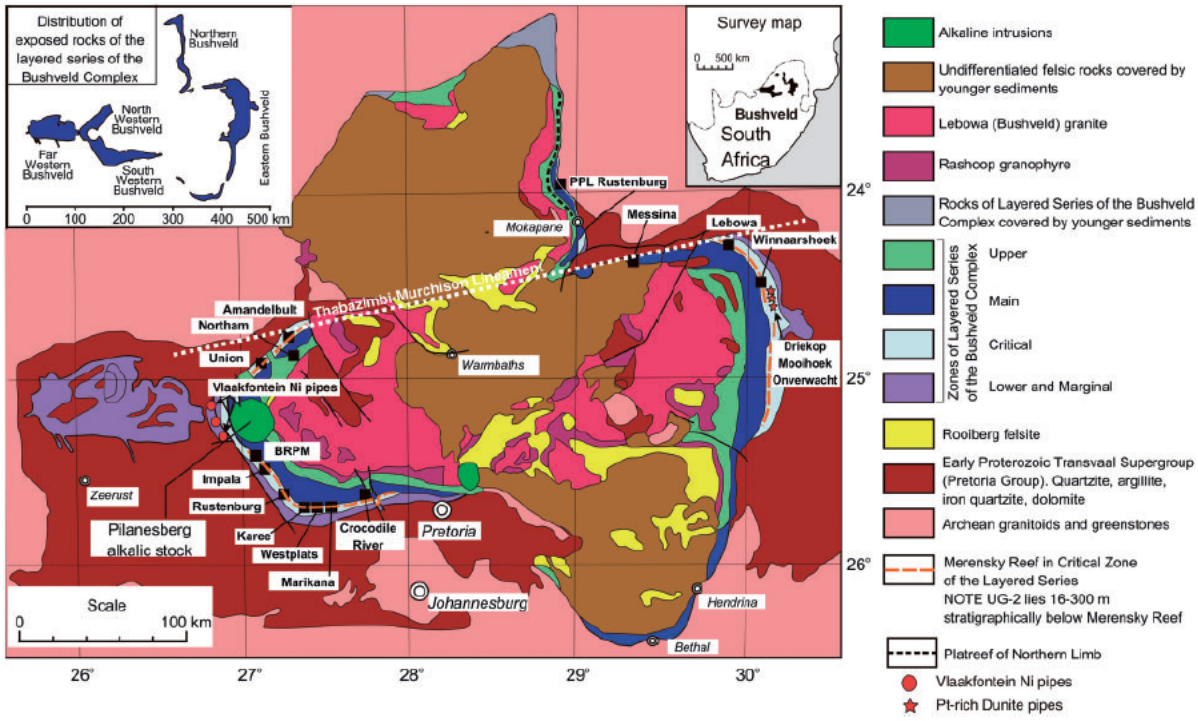

Figure 1.1: Geological map of the Bushveld Complex. Curtsey of Naldrett et al, 2009, who modified data by several sources provided by Eales and Cawthorn, 1996.

References

- Cawthorn, R.G., 1999, Permeability of the footwall cumulates of the Merensky Reef, Bushveld Complex: South African Journal of Geology, v.102(3), p.293-310

- Coghill, B.M., and Wilson, F., 1998, Platinum group minerals in the Selukwe subchamber, Great Dike Zimbabwe – Implications for PGE collection mechanisms and post-formation redistribution: Mineralog Mag., v.57, p.613-633

- Eales, H. V. and Cawthorn R.G., 1996, The Bushveld complex, Layered Intrusions: Elsevier Science B.V., p.181-229.

- Godel, B., Barnes, S.J. and Maier, W.D., 2006, 3-D Distribution of Sulphide minerals in the Merensky reef (Bushveld Complex, Soputh-Africa) and The J-M reef (Stillwater Complex, USA) and their relationship to Microstructures using X-Ray tomography: Journal of petrology, v.47(9), p.1853-1872.

- Godel, B., Barnes, S.J. and Maier, W. D., 2007, Platinum-group elements in sulphide minerals, platinum-group minerals, and the whole rock of the Merensky Reef (Bushveld Complex, South Africa): Implication for the formation of the reef: Journal of Petrology, v.48, p.1569-1604

- Merke, R.K.W., 1992, Platinum group minerals in the middle group of chromitite layers at Marikana, Western Bushveld Complex: Indications for collection mechanisms and post magmatic modification: Can. J. Earth Sci., v.29, p.209-221

- Naldrett, A. J., Wilson, A., Kinnaird, J. & Chunnett, G., 2009, PGE tenor and Metal Ratios within and below Merensky Reef, Bushveld Complex: Implications for its Genesis, Journal of Petrology, v.50(4), p.625-659

- Naldrett, A.J. and Von Gruenewaldt, G., 1989, Association with platinum group elements with chromitite in layered intrusions and ophiolite complexes: Economic Geology, v.84, p.180-187

2. Presentation of Paper

Experimental evidence for Sulphide Magma Percolation and Evolution: relevant to the chromite bearing reefs of the Bushveld Complex

C. Koegelenberg*, *L.M. Theron & G. Stevens*

Stellenbosch University Private Bag X1
Stellenbosch 7602 South Africa

Department of Earth Science

University of Stellenbosch

2011

***

Introduction

PGE mineralization in the Bushveld Complex is strikingly focused on the chromitite horizons of the Merensky Reef and the UG2. The mechanisms by which this association between chromitite and PGE concentration is achieved are not clear, yet it is thought that sulphide melt has an important role to play and that these horizons also mark the sites of new magma injections into the magma chamber (Cawthorn, 1999; Naldrett & Von Gruenewaldt, 1989). Two key issues relating to BC Pt mineralization are not well understood. The first of these is the details of the role played by the sulphide fraction of the magma. For example, if PGE's have been concentrated by the formation of immiscible sulphide liquids, why are the PGE concentrations in the reefs apparently too high to be easily reconciled with their sulphide contents (eg. Godel et al, 2007)? Similarly, if the Pt is sourced from silicate magma and concentrated by the formation of an immiscible sulphide melt, there is little evidence to suggest that the required large volumes of sulphide saturated silicate magma even existed (Cawthorn, 1999). The 1st observation has prompted several authors to argue that the reef horizons have lost sulphur, by sulphide mineral breakdown. The second major area of uncertainty relates to the origin of the chromitite layers. The solubility of chromium in basaltic liquid is very low, such that the magma volume represented by the preserved extent of the BC represents an insufficiently large reservoir to have crystallized the volume of chromite present. The Rustenburg Layered Suite (Union Section), on average, contains 0.38% Cr_2O_3. Experimental and empirical work indicates that more primitive liquids than those proposed to have formed the BIC have a maximum Cr_2O_3 solubility of less than 0.15% (Eales, 2000), and therefore lack the capacity to carry sufficient Cr_2O_3 in the dissolved state to crystallize the volume of chromite present. The lack of evidence for Cr-depleted residual liquids is argued to indicate that the magma chamber lost magma, however the volumes required to be lost are substantial. Mass balance requires a ratio 1:580m of monomineralic chromitite to the parental source liquid, and an even higher volume ratios would be required when considering incomplete extraction of Cr from the source liquid (Eales, 2000). The fact is, most mass balance issues regarding the source of chromite, sulphide and PGE in the complex are still to be resolved. However, these issues are central to understanding the mineralization mechanisms, explaining economic PGE distribution and producing refined exploration models.

Naldrett et al, 2009[a] states that variability of Pt/Ru and Pd/Ru, in relation to more consistent Ru/Os, Ru/Ir and Ru/Rh, in chromitite horizons indicate that Pt and Pd respond to different concentration mechanisms than other PGE. They argue the bulk of Pt and Pd were concentrated by sulphide liquid, while Rh, Ru, Ir and Os was concentrated by chromite itself, probably as grains of laurite and alloys incorporated in growing chromite crystals. Studies on the Merensky reef by Godel et al, 2006 & 2007 provide clues to how sulphide liquid, apart from scavenging Pt from silicate magma, could have affected Pt distribution. They propose that chromitite layers acted as a physical barrier or filter, trapping dense percolating

sulphide melts, partially contributing to Pt mineralization. This model is elegant, however the degree to which re-crystallised and annealed natural samples reflect the true sulphide melt silicate- and chromite-mineral interaction surfaces is uncertain. Sub solidus re-crystallization and re-equilibration of sulphide assemblages during cooling (Merke, 1992; Coghill & Wilson, 1998) completely transforms original, high-temperature sulphide textures and phases.

This process is experimentally testable under conditions of temperature and pressure relevant to the BC. In this study we aim to investigate three important aspects of sulphide magma behaviour: Firstly, we will investigate how sulphide melts wet chromite and silicate minerals. These wetting angles, also referred to as dihedral angles (Holness, 2005), of sulphide melt with chromite, silicate minerals and silicate melt control sulphide melt mobility through silicate and chromitite cumulates. Secondly, the window for effective fractionation of Pt in a two phase sulphide system, melt + Mss (mono-sulphide solid solution), within a sulphide composition relevant to the BC is poorly constrained. Consequently, this study will establish the phase relations, as a function of temperature. Thirdly, we investigate the consequences of chemical interaction between chromite and sulphide melt, in order to understand what changes percolation into chromitite layers will induce in the sulphide magma.

Geology of the Bushveld Complex

The Bushveld Complex is the world's largest known mafic to ultra-mafic layered igneous intrusion. The complex comprises of four distinctive igneous groups: Early mafic sills; the Rooiberg felsites, which form the roof over much of the layered sequence; the 8km thick Rustenburg Layered series (figure 1); and, the Lebowa Granite suite. The bulk of the PGE mineralization occurs within the Upper Critical zone, part of the Rustenburg Layered Suite (RLS). Apart from chromium, the Bushveld accounts for 75% and 37% of the world's production of Pt and Pd, respectively. Total PGM reserves are estimated at 63 million kg. This amounts to 95% of the world reserve. (Naldrett et al, 2009[b]). Generally, all chromitite layers in the RLS contain elevated concentrations of PGE, though the bulk of the PGE content occurs in 3 sulphide rich units; the UG2 chromitite accounts for 58% of Pt in the complex, the Merensky Reef for 32% and the Platreef for 10% (Naldrett et al, 2009[b]).

Throughout the RLS, continuous mineralogical evolution is attributed to fractional crystallization, as is reflected by changes in mineral assemblage and increasing Fe/Mg (figure 1) ratios within the ferromagnesian silicates (Seabrook et al, 2004). However this evolution is interrupted by regular shifts to a more mafic composition due to sporadic fresh magma impulses, hence the RLS comprises of several cyclic units. Magmatic cycles are observed as shifts in initial $^{87}Sr/^{86}Sr$ of the rocks (Figure 1) and in Mg# of olivine and pyroxene, and by sharply defined boundaries of ultramafic cumulate conformably/unconformably overlying less mafic cumulate. Models for both the formation of immiscible sulphide melt and chromitite layers, also considered as the primary PGE concentrators, are

mainly based on the mixing of evolved magma with "less" evolved magma (Campbell et al, 1983; Naldrett and Von Gruenewaldt, 1989; Li et al, 2001; Li and Ripley, 2005; Naldrett et al, 2009[a],[b]). As seen in the Critical and lower Main zones, the start of cycles are typically marked by chromite and pyroxenite horizons (Eales and Cawthorn, 1996; Cawthorn, 1999[a]), which include PGE, mineralized UG2 and Merensky reefs. Generally all chromitite layers are relatively enriched in PGE (Naldrett et al, 2009[a]), though not all are economically viable to mine.

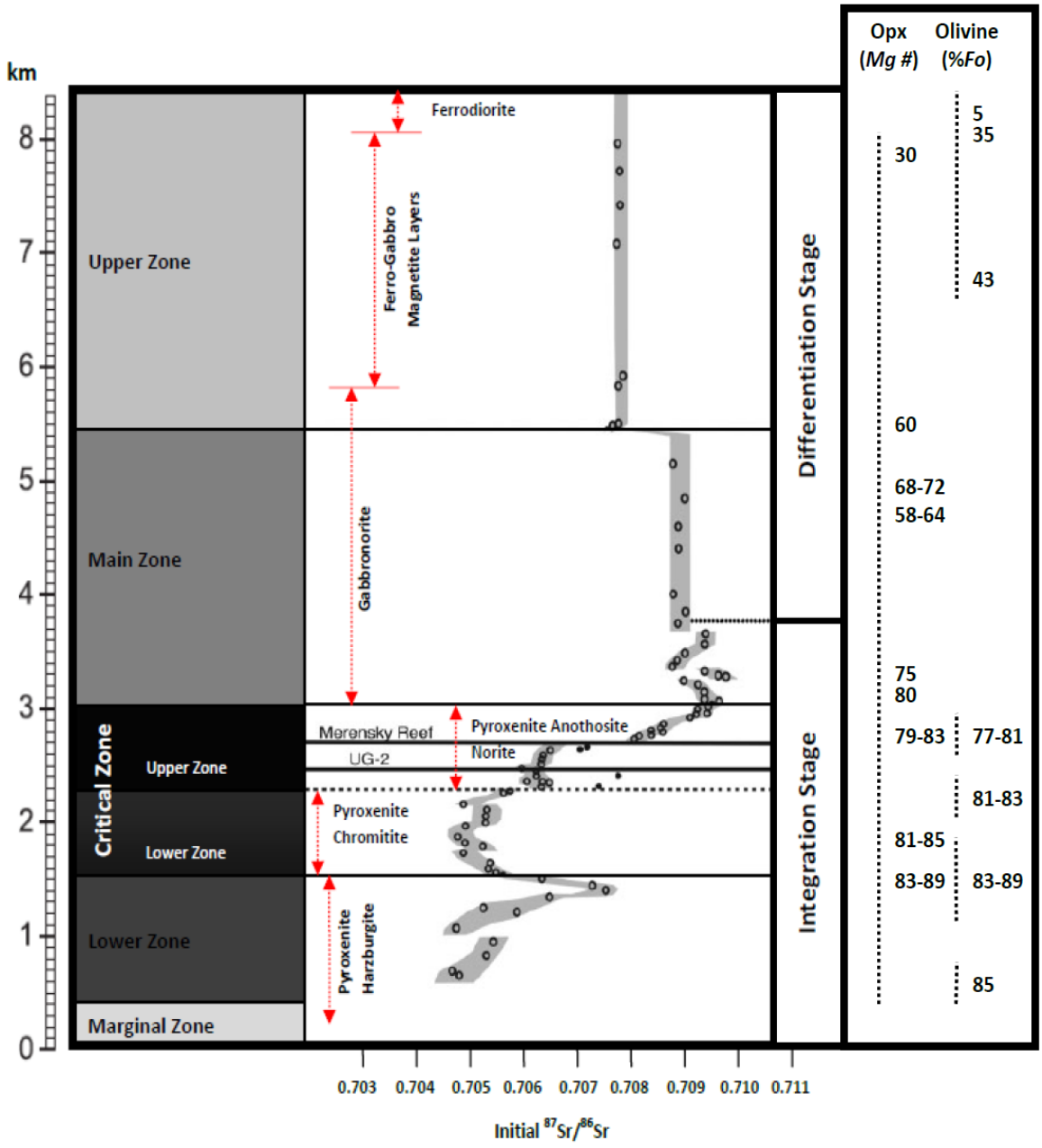

Figure 1: A schematic log section of the RLS, showing evolution of whole rock Sr^{87}/Sr^{86} initial isotopic ratios and lithology. The Mg# evolution caused by fractional crystallization is well observed in Ortho-pyroxene (Opx) and Fosterite (Fo). Modified after Kruger (1995); Naldrett et al, 2009; Eales & Cawthorn, 1996.

Sulphide melt as a collector of PGE

The concentration of PGE in immiscible sulphide melt revolves around two primary parameters: firstly, preferential partitioning of PGE between sulphide melt and silicate melt and secondly, the ratio of sulphide saturated magma in equilibrium with immiscible sulphide liquid (R-factor) Cambell & Naldrett, 1979). Extremely high $D_{sil/sulp}$ values are supported by experimental data, but in detail, the D values determined in different studies are somewhat inconsistent. Experimental data by Bezmen et al, 1994 calculated a $D_{sil/sulp}$ value of 10^6 however, Tredoux et al, 1995 and Fleet et al, 1996 summarize the problems associated with the interpretation of such experimental results and argue that $D_{sil/sulp}$ will not greatly exceed 10^4. Modelling Pt concentrations in sulphide assemblages with the same $D_{sil/sulp}$ and R-factor for chromitite and hanging wall melanorite layers yield contrasting results (eg. Godel et al, 2007). Even though Pt concentrations within sulphide in chromitites are typically double those of sulphides in the hanging wall melanorites, the volume of sulphides in chromitites appears to be insufficient to account for the bulk rock Pt. Consequently, the additional Pt, unaccounted for by sulphide, is believed to exist as PGM crystallised before sulphide saturation. In contrast, sulphide volumes in the hanging wall melanorites are sufficient to account for Pt (Godel et al, 2007). However, these calculations do not take into account Pt fractionation between Mss and sulphide melt. The influx of an evolved sulphide melt with an extremely high Pt concentration, into a particular chromitite horizon will significantly increase the apparent $D_{sil/sulp}$ or R-factor required to account for Pt mineralization.

Nevertheless, to account for all PGE within a specific cycle, the small volumes of sulphide liquid implied by the relatively low sulphur content of the reefs, and the low inherent PGE solubility within appropriate silicate magma compositions (Cawthorn, 1999[b]), require equilibration with an enormous volume of sulphide saturated silicate magma as the source of PGE. Therefore the Merensky and UG2 chromitite are considered to be extremely high R deposits (R>>D). However, as stated Cawthorn, 1999[b], it is impossible to accurately determine R for any geological cycle or processes, thus it can only be argued, that the enormous size of the Bushveld magma chamber had the capacity to permit processes to operate with large R-values. This concept appears to be at odds with the fact that the rocks associated with the reef horizons record chemical variability best reconciled with successive injections of new magma and within layers that appear not to record sulphide melt saturation. Insufficient sulphur in hanging- and footwall cumulates within a few meters relative to the Merensky and UG2, strongly argues that large volumes of sulphide saturated magma probably never existed (Cawthorn, 1999[b]). Despite these apparent shortfalls, the association of chromite, as layered chromitite horizons, and sulphide with Pt is a clear phenomenon (Naldrett et al, 2009[b]), as is illustrated in figure 2.

Extreme Pt/S in Chromitites

To explain extremely high Pt/S ratios in chromitites, as illustrated in figure 2, it is

generally argued that the re-equilibration of chromite crystals caused the destruction of interstitial sulphide. According to this hypothesis (Naldrett et al, 2009[a]), vacancies in chromite minerals above 900^{O}C could be filled by Fe^{2+} sourced from interstitial sulphide. They propose that affected sulphide becomes oversaturated with S and releases sulphur gas via the following reaction:

$$^{3}/_{4}\,(Fe_2O_3) + {}^{1}/_{3}\,(FeS) = Fe_3O_4 + {}^{1}/_{6}\,(S_2)$$

Naldrett and Lehmann, 1988, further argue, by considering fO_2, of a wide range of basalts that this process may account for the apparent sulphur deficiency relative to Pt in chromitite layers. However, selenium (Se) substitutes for S in sulphides, hence the loss of S can be evaluated by comparing whole rock S/Se ratios with primary magmatic S/Se (~3000) (Lorand et al, 2003). S is more mobile during alteration than Se and consequently the S/Se ratio should decrease when S is lost (eg. ~1400 for the J-M reef, Stillwater Complex; Godel et al, 2006). Merensky reef S/Se ratios range between 2500 - 3000 (Godel et al, 2007; Barnes and Maier, 2002) and does not indicate extensive loss of S. Consequently, it seems unlikely that extreme Pt/S ratios in chromitites are caused by the loss of S.

Alternatively, extreme Pt/S in chromitites could be caused by; firstly, chromitite layers acting as a reservoir for evolved sulphide melt within which Pt concentrations have been increased due to fractional crystallization of MSS. This would require sulphide melt to crystallize substantial Mss in the hanging wall melanorite creating a fractionated Ni and Cu rich sulphide melt. This evolved melt, according to Godel et al, 2006, should be trapped by chromitite layers. Experiments show that Pt is highly incompatible within high temperature Mss and partitions strongly into the sulphide melt phase, with D_{Pt} as low as 0.01 (Ballhaus et al, 2006; Wohlgemuth-Ueberwasser et al, 2007; Theron et al, in preparation). In general sulphide assemblages in chromitites are much higher in % Cu, %Ni and ppm Pt (Figure 2) than adjacent hanging wall melanorite layers. Considering that evolved sulphide melts have significantly higher Cu and Ni concentrations (Ballhaus et al, 2006; Theron et al, in preparation; Kullerud et al, 1969; Fleet and Yuanming, 1994) compared to coexisting Mss, the common anomaly of high Cu, Ni and Pt concentrations in chromitites, relative to S, indicates that sulphide mineralization in chromitites were arguably caused by high proportions of Pt rich sulphide melt. Of course this does not answer the primary question of how the original Pt-rich sulphide magma is produced; all the R-factor based problems discussed above still apply.

Secondly, Pt solubility in sulphide melt decreases markedly with lower S concentrations (Peregoedova et al, 2004; Li et al, 1995) and can cause Pt alloys to crystallize from a sulphide melt, with roughly 0.4 – 0.5 wt% PGE, at temperatures in excess of 980^{O}C. Crystallizing Mss not only reduces the S content of sulphide melts, but also decreases sulphide melt volume (Theron et al, in preparation). Consequently, the continued crystallization of Mss causes a gradual decrease in S content coinciding with Pt enrichment (due to preferential partitioning) of sulphide melt. It seems

likely that evolved sulphide melts crystallizing Pt alloys within chromitite layers and the percolating out of the layer could contribute to high Pt/S ratios within the layers. Detail analysis of PGM distribution within the Merensky Reef and associated rocks (Godel et al, 2007) indicates that 75% of PGM in the chromitite occur at the chromite/silicate sulphide mineral interfaces and 7% occur as isolated inclusions either in chromite or silicate. The rest of the 18% PGM is included in sulphide. In contrast, for melanorite and anorthosite layers, 40% of PGM occurs as interfacial crystals associated with sulphides, 14% as isolated inclusions within plagioclase and 46% as inclusions in sulphide. Importantly, of all the PGM in chromitite, 63% is Pt-Pd sulphide, compared to only 5% Pt-Pd in the silicate (Godel et al, 2007). The distribution of PGM, in particular Pt-Pd, in chromitites, does resemble patterns to be expected if PGM crystallized or Pt alloys formed, from sulphide melt. However this has always been questionable considering the unavoidable re-crystallization of the sulphide material at lower temperatures.

Thirdly, Finnigan et al, 2008, show that chromite crystallization could concentrate PGE directly from the silicate magma prior to sulphide saturation. By modelling the transient perturbation of fO^2 between chromite and PGE saturated silicate melt at 1Atm ($1400^{O}C$), they observed the precipitation of interfacial PGM's during growth and diffusive re-equilibration of chromite (Cr-spinel) with silicate melt. Local reduction of silicate melt via the selective uptake of trivalent Fe and Cr relative to the divalent species by chromite causes a significant drop of PGE solubility in the silicate melt in the mineral-melt interfacial region (Finnigan et al, 2008). This could trigger the formation of Pt alloys, which will result in higher Pt/S for chromitite layers. However, to form IPGE (Os, Ir, Ru) alloys, newly crystallized or equilibrating chromite grains would require interaction with a large volume of basaltic silicate magma close to being saturated with IPGE.

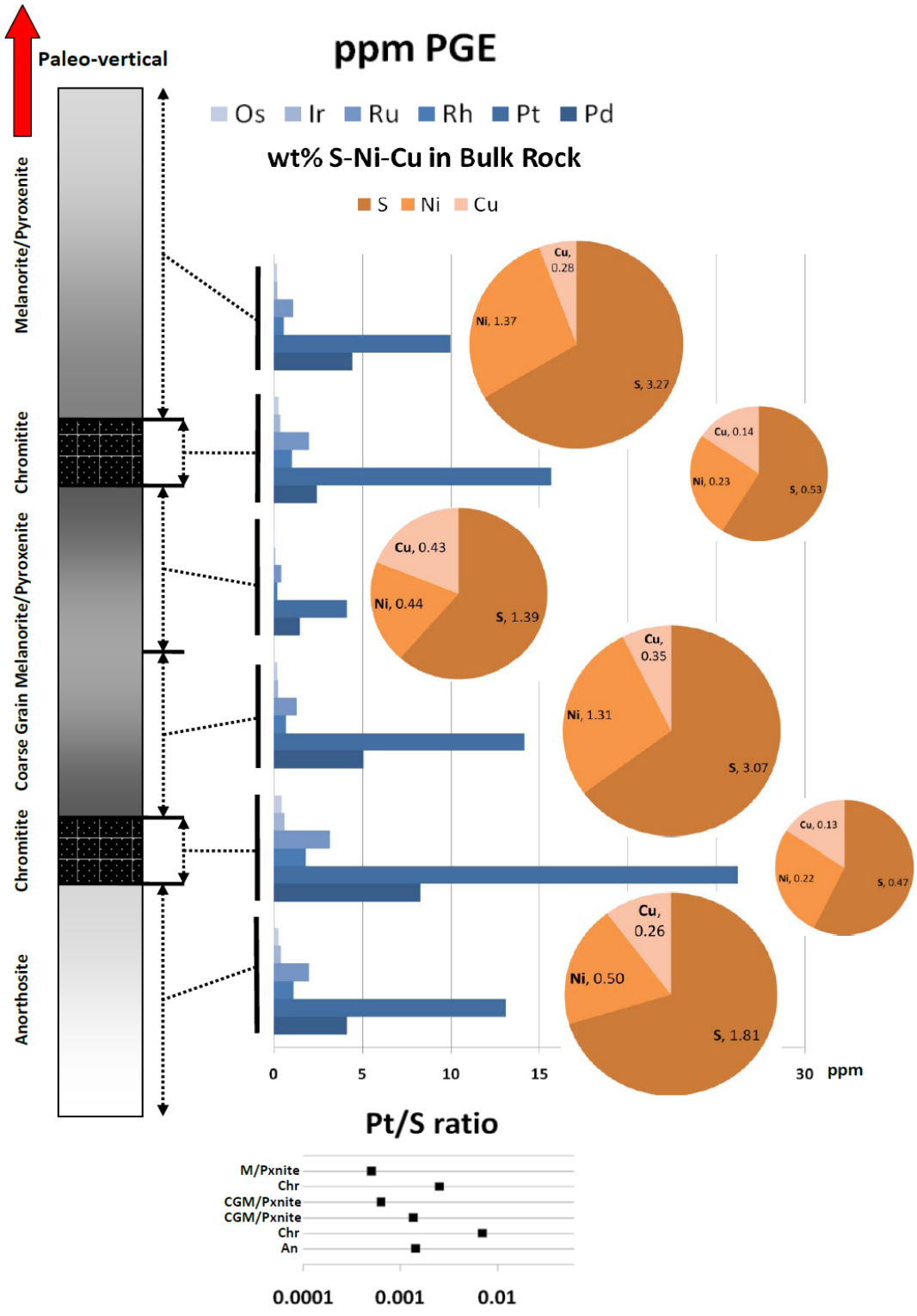

Figure 2: An illustration of a normal Merensky reef section, showing PGE tenor, Pt/S and bulk rock Cu, Ni and S wt%, with respect to lihological stratigraphy. Data from Naldrett et al, 2009 and Godel et al, 2007. No particular reference towards the vertical extent of a Merensky cyclic unit is made, due to a variation in thickness from several cm to close to 1m.

Sulphide Melt Wetting

The relative wetting properties of melts on minerals can be quantified as measured dihedral angles. The angle created at the junctions of two solid crystal grains in textural equilibrium with a fluid phase, is known as the fluid-solid-solid dihedral angle (Holness, 2005). The relative magnitude of energy of grain boundaries and that of fluid-solid interfaces controls the dihedral angle via the following equation:

$$\sum_{i=1}^{3}\left(\gamma_i t_i + \frac{\partial \gamma_i}{\partial t_i}\right) = 0$$

where $\gamma_1, \gamma_2, \gamma_3$ are the three interfacial energies, t_i is the vector in the plane of the ith surface, normal to the line of intersection of the surfaces and pointing away from this line, and $\frac{\partial \gamma_i}{\partial t_i}$ is a vector perpendicular to t_i and to the line of intersection (Herring, 1951). Simply, this equation defines the orientation of the interfaces at three-phase junction or pore corner.

The connectivity of sulphide melts in a solid matrix (eg. Crystals) is controlled by the relative energies of crystal-crystal and crystal-melt interfaces (Godel et al, 2006). By considering surface energies to be isotropic for the solid matrix in which the sulphide melt resides, it is possible to predict sulphide melt topology by considering dihedral angles. At a dihedral angle of less than 60^0, the melt is considered to wet the crystal faces, even at low melt fractions and porosities (Smith, 1964; Bulau et al, 1979; Watson, 1982). Where dihedral angles are more than 60^0, interconnectivity is not achieved and melt is considered not to wet crystal surfaces at low melt fractions (Holness, 2005). Crystallographic orientation has a effect on dihedral angles, however in realistic systems with some anisotropy of interfacial energies, systems still have dihedral angle percolation thresholds of $<=60^O$ at porosities of a few percent (Minarik & Watson, 1995; Wark & Watson, 1998).

Other parameters controlling sulphide liquid mobility, involve mostly density, viscosity and grain size, but most importantly, the presence of silicate melt. Despite sulphide liquid being very dense (4000 $Kg.m^{-3}$, Kushiro et al. 1976), it has a very low viscosity of 0.01 Pa.s compared to Merensky reef silicate magmas of 100-1000 Pa.s (Cawthorn, 1999*). As a result, less dense silicate melt will wet the outside of sulphide melt resulting in isolated droplets of sulphide melt roughly 1.5µm in size (Bockrath & Ballhaus, 2002). However, dihedral angle would be the prime parameter controlling the connectivity of fluids, hence an indication of the permeability of the sulphide liquid/melt bearing rock.

Experimental Sulphide phase relations

Relevant sulphide phase relations have mainly been studied at 1 atm, however it is estimated that the Bushveld Complex intruded at pressures of ~4 kbar (Nell, 1984). The effect of a pressure increase from 1 atm to 4 kbar on the sulphide solidus is roughly a 30^OC-40^OC increase for sulphide systems with an atomic

metal/S ratio of 0.93 to 1.06; for metal/S ratios >1.11, the solidus is characterised by no apparent pressure dependence (Ballhaus et al, 2006). Thus, we assume that sulphide phase relations determined at1 atm are very close to being accurate for the BC.

Sulphide magma evolution within the BC can largely be understood by extrapolation from the Fe-Ni-S, Cu-Fe-S, and Cu-Ni-S ternary systems (Kullerud et al, 1969). Current BMS assemblages of pentlandite, pyrrhotite, chalcopyrite and pyrite in the BC do not resemble the sulphide assemblage at high temperature (>800^{O}C) which consists initially of Mss and possibly Iss (intermediate-solid-solution), (Kullerud et al, 1969; Fleet and Yuanming, 1994). Figure 3 illustrates typical 1atm sulphide phase relations with added PGE at 980^{O}C–1000^{O}C. The maximum thermal stability for Mss is at 1190^{O}C and is defined by a composition along the Fe-S join with 48 atomic % Fe (Naldrett, 1989). Thus, during cooling, the first phase to crystallize out of sulphide melt is Fe rich Mss, $(Fe, Ni)_{1-X}S$. Increasing Ni and Cu content of the system decreases the solidus temperature. However in a Fe rich sulphide system, similar to that observed in the Bushveld, Cu and Ni never exceed 6 and 22 atomic % respectively (Fleet and Pan, 1994). Iss, $(Cu, Fe)S_{1-X}$, is only stable below temperatures of approximately 950^{O}C (Fleet and Yuanming, 1994) with a composition (atomic %) of 30.1% Fe, 24% Cu and 45.9%. Only after crystallization of Mss, will the residual sulphide melt be likely to crystallize as Iss. Thus, during high temperature crystallization, the sulphide magma would have consisted of Mss co-existing with a sulphide melt enriched in Cu and Ni. Additionally, Fleet and Yuanming, 1994 indicates sulphide melt has consistently lower S concentrations than Mss (up to 2.1 at% less S, 1050^{O}C) and that this difference increases at lower temperatures with up to 6 at% less S in the melt than in Mss at 850^{O}C. Thus, collectively these findings predict that fractional crystallization of Mss from sulphide magma drives the melt towards more Ni- and Cu-rich, and S-poor compositions. Inevitably this trend decreases Pt solubility within melt and Mss and formation of Pt alloys will occur (figure 3).

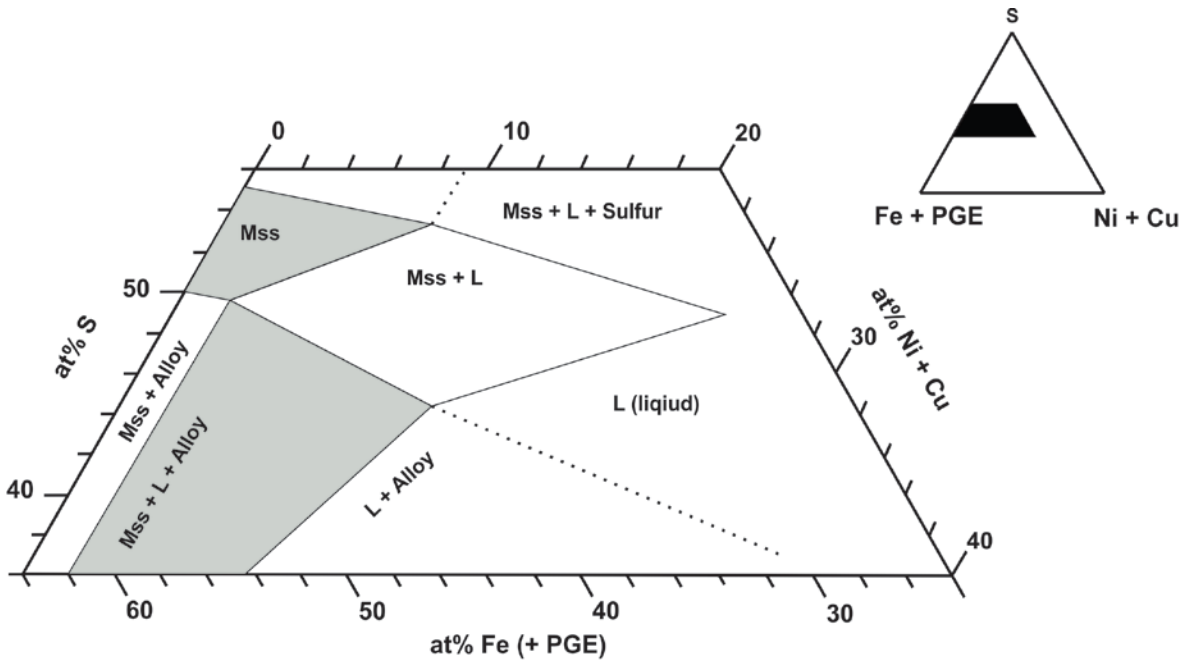

Figure 3: Sulphide phase relations in the 1atm Fe-Ni-S, Cu-Fe-S, and Cu-Ni-S ternary system with 0.4 - 0.5 wt% PGE added at 980^{O}C-1000^{O}C. (After Peregoedova et al, 2004). Note: no Iss at >950^{O}C.

Sulphide Experiments

Sulphide composition: Previous experimental studies (Fleet and Yuanming, 1994, Ballhaus et al, 2006) that have investigated sulphide melting phenomena relevant to the BC have used a wide range of compositions that differ from both average BC sulphide compositions and the likely composition of any sulphide melt that may have been introduced into the magma chamber directly from the silicate magma source. The compositions of sulphide melt produced by sulphide saturated mantle melting events (eg. Bockrath et al, 2004) are similar to the bulk sulphide composition of the BC (eg. Godel et al, 2007), suggesting that sulphide melt may be of direct mantle origin. Studies of the sulphide melt composition produced within the upper mantle (Bockrath et al, 2004), indicate a sulphide melt composition of 36.5 at% Fe; 8.95 at% Ni; 3.29 at% Cu; and 51.3 at% S. Ni concentration was calculated assuming that the sulphide melt to be in equilibrium with upper mantle olivine containing 90 mol % forsterite and 3000 parts per million (ppm) Ni; the Cu concentration assuming that 50% of the Cu in primitive mantle (~20 ppm) resides in the sulphide assemblage. Atomic metal/S was set to 0.93, reflecting a sulphide in moderately oxidized mantle in equilibrium with the fayalite-magnetite-quartz oxygen fugacity buffer (Bockrath et al, 2004). This composition is very close to the proposed bulk sulphide composition of the Merensky reef (35.4 at% Fe; 9.86 at% Ni; 5.18 at% Cu; and 49.4 at% S, Godel et al, 2007). In this study we use the composition estimated by Bockrath et al, 2004, as a suitable starting sulphide composition that we propose is directly relevant to the formation of the Bushveld ores.

The concentration of Pt in the sulphide starting material was restricted to between 100ppm-150ppm to ensure trace element behaviour of Pt, whilst still being within the analytical capabilities of a SEM WDS detector within the phases where Pt has concentrated. Normalized to 100% sulphide + Pt, bulk Pt concentrations in the Merensky reef sulphide range from 906ppm to 2495ppm in the upper and lower chromitites, and 496ppm to 228ppm in coarse grained melanorites (Godel et al, 2007). However in the hanging wall melanorite Pt concentration within sulphide ranges from 100ppm to 189ppm. Thus we regard 100ppm-150ppm Pt to be a reasonable lower estimate of the range of Pt concentrations of relevance to the sulphide melt that contributed to ore formation in the BC.

Synthesis of the Starting Material: Synthetic Cu-Ni-Fe mono sulphide was prepared for use as the starting material by combining powders of S, Fe, Ni, Cu and $PtCl_2$ (36.9 wt% S, 4.7 wt% Cu, 11.8 wt% Ni, 45.7 wt% Fe + 100ppm Pt) in a 12mm pyrex tube, before it was flushed with argon, evacuated, then sealed with oxy-acetylene torch to prevent unwanted oxide phases from forming. Trace amounts of boron-nitride were also added to the mixture to scavenge any remaining oxygen (process similar to that of Ballhaus et al, 2006). The tubes were suspended in the hot zone of a vertical tube furnace and baked at $1200^{O}C$ for 2 hours. According to studies by Ballhaus et al, 2006, $1200^{O}C$ is well above the 1 atm liquidus for the Cu-Ni-Fe mono-sulphide system. The tubes were quenched instantly by dropping into a water bath at $15^{O}C$. This yields a relatively homogeneous frozen sulphide melt. Note that sulphide melt does not quench completely homogeneously (Ballhaus et al, 2006) and quench crystals are always produced, as illustrated by figure 4. However, the rapid quench rate ensures that the crystals are very small and intergrown. Consequently, analysis of areas as small as $400\mu m^2$ produces representative compositions of bulk compositions. The starting material was ground in an agate mortar under acetone (preventing oxidation) for several minutes down to a grain size of approximately 10µm (measured with SEM). The fine sulphide material was then preserved under vacuum in a desiccator prior to use in the experiments.

1Atm Experiments: Experiments at atmospheric pressure are crucial to this study, in that they allow for extremely fast quenching. Fast quenching yields textures where the quench crystallised melt is relatively easy to distinguish from crystals of Mss that coexisted with melt at the temperature of equilibration. Consequently the equilibrium assemblage of phases (Mss + sulphide melt) is easier to identify in these experiments than in runs at high pressure where the quench rates are at least an order of magnitude slower. Two different types of experiments were performed. Firstly, experiments containing only the sulphide starting material were performed to investigate phase relations in the sulphide system. Secondly, experiments were performed where sulphide melt or magma was allowed to interact with a volumetrically dominant chromite powder. These experiments were conducted to investigate reactions between chromite and sulphide melt and the possible effect of this on the composition of sulphide melt.

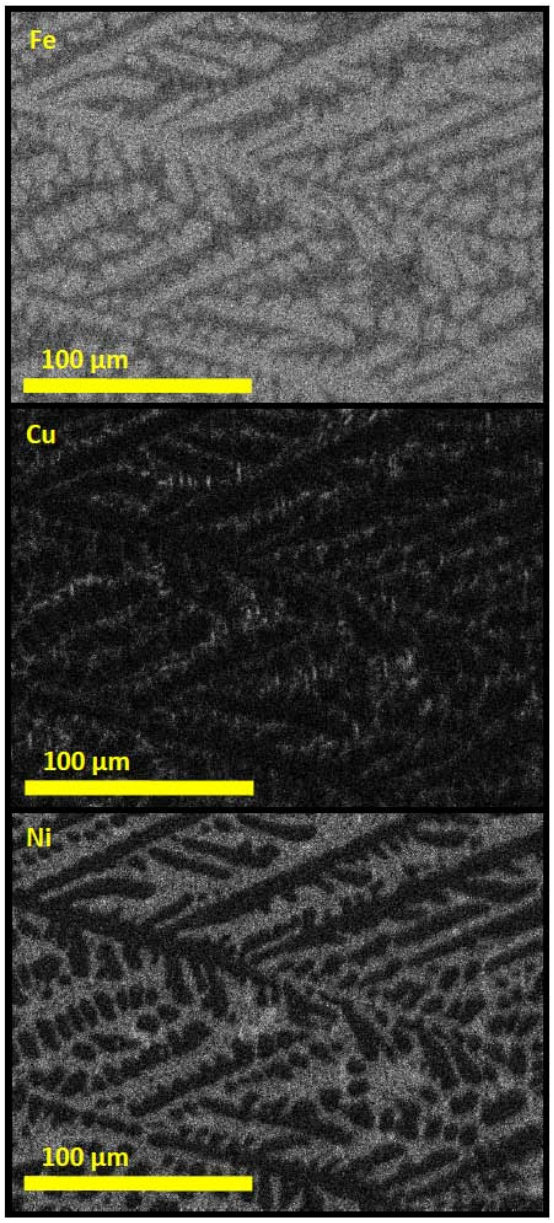

Figure 4: *SEM gray scale X-ray maps of the quenched sulphide melt synthesised at 1200^{O}C and 1Atm. Large pools of quenched melt are characterised by a dendritic intergrowth pattern consisting of quenched Mss, high Ni and Cu phases. Fe partitions strongly into quench crystallised Mss, while Ni and Cu remain in the residual melt for longer.*

The experimental procedure for the 1Atm runs is similar to that used to synthesize the staring material (discussed previously). However, instead of using elemental powders, small (<<0.1g) portions of synthetic mono sulphide are used and sealed in a much smaller 6mm pyrex tube. The smaller sample size allows for even faster quenching (<<1s). To ensure complete homogenization of sulphide melts, charges were heated to 1200^{O}C and held at that temperature for 30 minutes. Following this, they were cooled at a rate of 3^{O}C/min to the intended temperature of the run and left to equilibrate for 5 hours. The short run times, compared with typical silicate phase equilibrium experiments, are supported by results of Barton, 1970, who concluded that Cu-Fe sulphide systems equilibrate within hours, even at temperatures as low as 400^{O}C. Typical silicate systems at 800^{O}C equilibrate over a period of several days to weeks, (e.g. Stevens et al, 2005). The quench method is identical to that used in the synthesis of the starting materials. Experiments in the chromite-free sulphide system were conducted at 850, 900, 950, 1000 and 1050^{O}C.

The experiments with chromite added contained 10% of the sulphide starting material and 90% crushed chromite powder. Chromite material was sourced from a Merensky reef sample from Rustenburg Platinum Mines (RPM), Union section, Zwartklip facies in the North-Western Bushveld Complex. Two experiments of this type were conducted at 1000^{O}C and 1150^{O}C. These were intended to bracket the sulphide liquidus in this system which is estimated to be located at 1050^{O}C (Theron et al, in preparation).

4Kbar Experiments: Experiments were conducted at pressure in order to investigate the physical interaction of sulphide melts with a synthetic cumulate containing a chromitite layer within layers

of super-solidus pyroxene dominated silicate magma. Thus, these experiments aim to study the wetting properties of sulphide melt in contact with chromite, pyroxene and silicate melt. Additionally, the rate of sulphide melt percolation through such layered structures, as well as possible compositional changes in sulphide melt (due to reaction with surrounding minerals) will also be analysed.

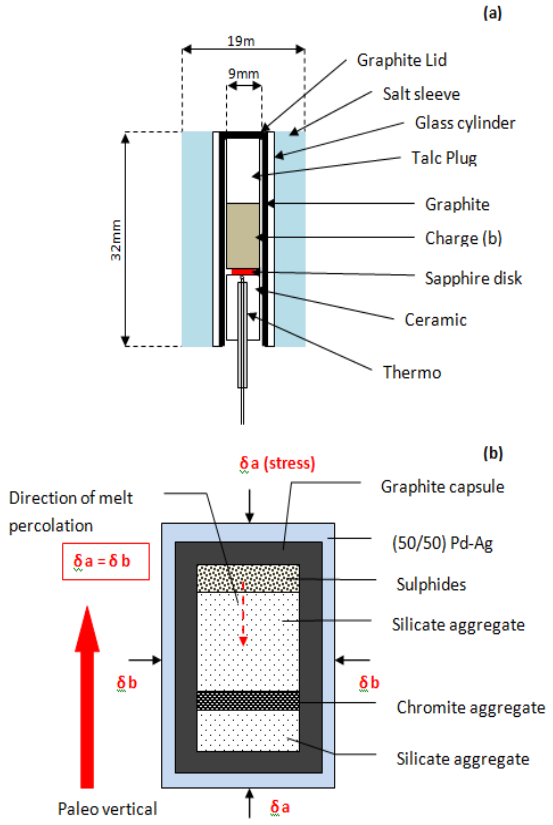

Figure 5a: 19mm pressure cell design. **b:** 4Kbar experimental charge design.

Starting materials for these experiments include the synthetic sulphide material, chromite and pyroxene-plagioclase aggregates derived from the same Merensky reef sample used as the source of chromite in the 1Atm experiments. Minerals were separately ground to powders for several minutes till a grain size of ideally <30µm (measured with SEM). The chromite powder was kept pure to simulate a chromitite layer, however the silicate powder consisted of a mixture of 50% pyroxene and 50% feldspar, similar in mineralogy to the coarse grained melanorite of the Merensky reef. The experimental charge consisted of a horizontally layered core of silicate, chromite and synthetic sulphide encapsulated with graphite and Pd-Ag alloy. The sulphide layer was placed on top of the layered silicate-chromitite package (figure 5b). The outer sealed and malleable Pd-Ag capsule ensures a closed system whilst the inner graphite capsule minimizes sulphide interaction with the Pd-Ag alloy.

High pressures were achieved in a Hollaway design non-end-loaded 19mm piston cylinder apparatus (figure 5a). All experimental charges were slowly compressed until stable at 4Kbar. Separate experiments were performed at 1100^{O}C, 1050^{O}C, 1000^{O}C, 950^{O}C and 900^{O}C. Run times varied from 24h to 96h before quenching. Quench rates were enhanced by a compressed cold water (18^{O}C) cooling jacket, enabling quench rates of approximately >500^{O}C/min. Type-K thermocouples, located at the base of the charge where used to monitor the temperature. When compressed the charge has a vertical extent of 4-5mm, and according to previous study by Stevens et al, 2005, using the same apparatus and a 13mm pressure cell, the vertical temperature gradient for a similar size charge does not exceed 10^{O}C. The run products consisted of solid cylinders of silicate, chromite and sulphide (Mss) layers with interstitial sulphide melt together with small volumes of interstitial silicate melt.

Analytical Methods: Experimental run products consisting of the entire capsule (figure 5b) were preserved in an epoxy mould and cured under vacuum to limit oxidation. Moulds were sanded down to half thickness, producing samples with vertical sections through the capsules and run products. Preparation of samples for scanning electron microscope analysis started with sanding using a sequence of 360, 600 and 1000 grade grit, followed by a polishing sequence involving 20µm, 9µm, 3µm and 1µm laps. All the image generation, elemental mapping, dihedral angle measurement and quantitative analysis were performed using a Zeiss EVO MA15VP scanning electron microscope (SEM). Images were produced by BSE (Back scattered electron) mode and both point and area quantitative analysis was performed using Energy dispersive X-ray spectrometer (BSD detector) and Genesis XM2 software. For analysis, EHT was 20kV with a working distance of 8mm. For chromite and sulphides, the analyses were standardized using commercially available natural sulphide and chromite mineral standards. Analysis of marcasite, pentlandite and cuprite of known composition indicated that typical uncertainties for elements analysed were 0.20 wt% for Fe, 0.14 wt% for Ni, 0.63 wt% Cu and 0.14 wt% for S. For chromite compositions, analysis of chromite and illmenite of known compositions indicated uncertainties of 0.05 wt% for Fe, 0.40 wt% for Cr, 0.08 wt% for Al, 0.16 wt% for Mg and 0.10 wt% Ti.

Results

1Atm Sulphide phase relations: Phase relations at 1atm are relatively easy to interpret due to the extremely fast quenching achieved in these experiments. This minimizes the size of the quench crystals that form from the melt, allowing melt domains to be easily distinguished from Mss that was stable at the experimental conditions. These relations, despite being at 1atm, can be applied to the relatively slow quenched 4kbar experiments considering that the raise in pressure only increases the Mss solidus by roughly 30^{O}C-40^{O}C (Ballhaus et al, 2006). Figure 6 illustrates the assemblages and textures produced in these experiments. Mss and sulphide melt coexist between 900^{O}C and 1150^{O}C (figure 6A and 6C). Mss has no crystalline shape/orientation and forms rounded, ball like shapes. Sulphide melt, although consisting of multiple quench phases, is always interstitial between relatively large MSS crystals or accumulations of crystals.

Given that sulphide melt becomes more Ni and Cu rich as a function of decreasing temperature, we expect quench phases produced from sulphide melt to change as a function of temperature of experiment, as this controls both melt composition and melt proportion. Comparing figure 6a to 6c, there is marked difference between quench textures at >1000^{O}C (6c) and 950^{O}C (6a). At >1000^{O}C the more Fe-rich melt is still concentrated enough with Fe to crystallize additional quenched Mss together with a quench phase concentrated in Ni and Cu. However, at 950^{O}C, the melt is more depleted in Fe and S, while being richer in Cu and Ni. Quench phases include a Ni-rich phase and a separate, interstitial Cu-rich phase. Importantly, during quenching, the sulphide melt quench crystallises according to a predictable sequence. The typical sequence

involves firstly, if sufficient Fe is available, the crystallization of quenched MSS followed by the crystallization of a Ni phase, while the remaining residual melt freezes as a Cu rich phase. In figure 6B, Pt alloys crystallized on the outside rim/border of equilibrium MSS crystals at 950^{O}C. This indicates that Pt alloys crystallised prior to the complete solidification of sulphide melt and therefore had to occur above the sulphide melt solidus. The predicted solidus for this BC relevant Fe-Ni-Cu-S system is at 800^{O}C (Theron et al, in perparation), thus Pt alloy crystallization should not be regarded as just a low temperature phenomenon, even for a sulphide system with conservative Pt concentration of (100-150ppm). Importantly, within BC sulphide compositional parameters it is likely that Pt alloy formation occurred in conjunction with mobile sulphide melt phases.

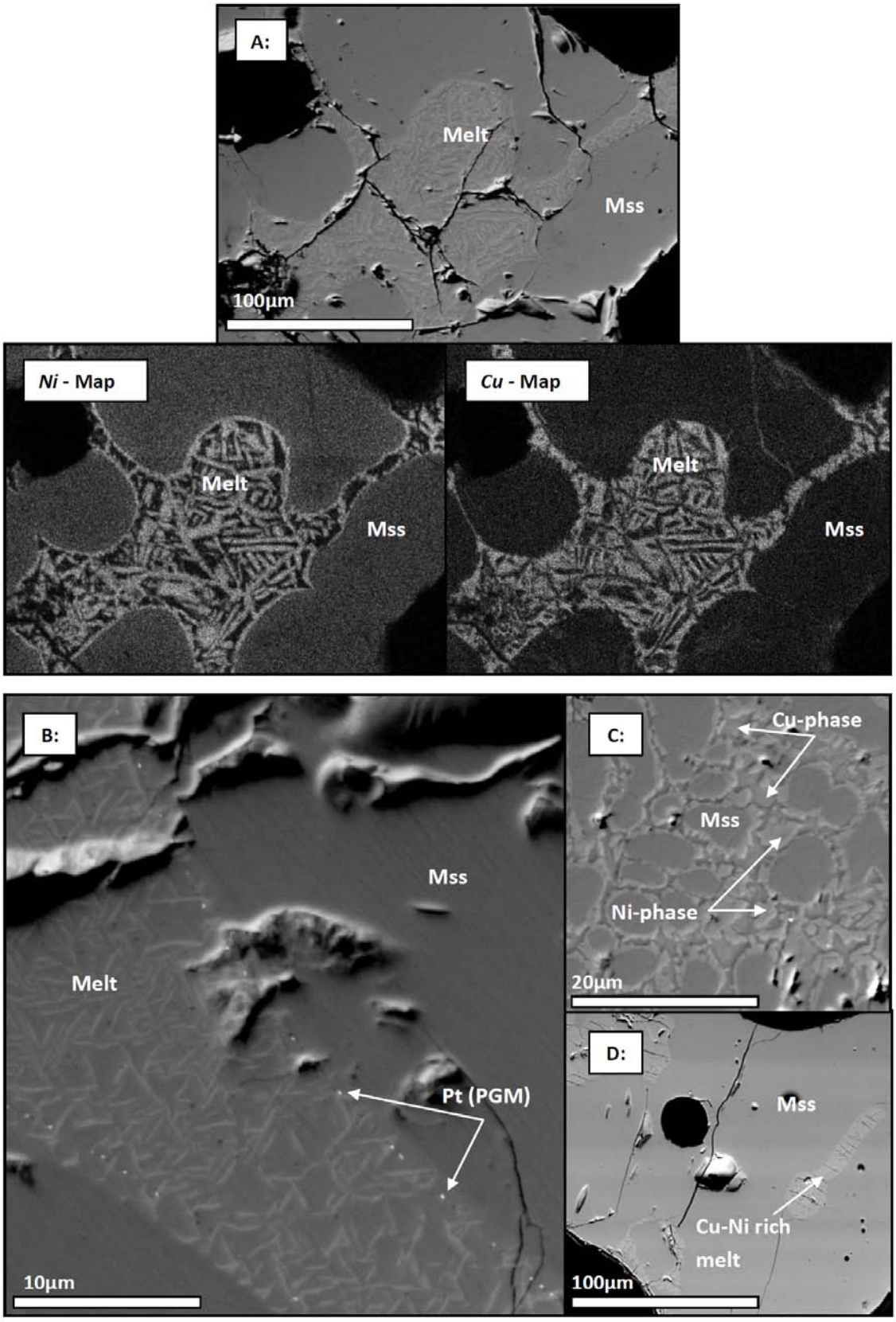

Figure 6: A) A BSD image together with X-ray Ni and Cu elemental maps showing equilibrium MSS and sulphide melt at 950^{O}C (1atm). **B)** At 950^{O}C (1atm) quenched sulphide melt crystallizes Pt (PGM) on the border of equilibrium MSS. Quenched sulphide melt

composes of a crystalline Ni rich, needle like phase and a interstitial Cu rich amorphous phase. **C)** Typical sulphide melt quench textures at >1000^{O}C (1atm). Phases include small MSS crystals which are overgrown by a highly Ni concentrated phase, while a phase highly concentrated with Cu resides interstitially. **D)** Slow quenched sulphide melt (>1000^{O}C) is dominated by crystallizing MSS, isolating late Ni and Cu rich residual melt into pockets, resulting a heterogeneous frozen melt.

4Kbar Textural Analysis: These experiments were designed to investigate the interaction of sulphide melt with silicate and chromitite layers. At 1100^{O}C the sulphide fraction was completely molten, however between 1050^{O}C to 900^{O}C, the sulphide system was partially molten consisting of melt + Mss. Figure 7 illustrates typical assemblages and textures produced in both long- and short-duration high pressure experiments. The silicate and chromite fractions of the starting materials of experiments at temperatures between 950^{O}C and 1050^{O}C have partly to completely re-crystallized textures after 96h. Silicate minerals are completely re-crystallized with plagioclase showing the most annealed texture filling interstitial space between pyroxene minerals (figure 7d). Chromite was slower to re-crystallize and in the 24h experiments retained a much more angular texture (figure 7a) than the silicate minerals. During the long duration experiments (96h) chromite minerals are completely re-crystallized and as a result coalesce due to new growth boundaries (figure 7c). Both sulphide and silicate melts are produced in the experiments and these are always interstitial (figure 7d). However, silicate melt volume is negligible below 1000^{O}C. When the silicate melt volume exceeds that of the sulphide melt, silicate melt wets the outside of sulphide melt creating isolated droplets (figure 7d). The percolation of sulphide melt needs space to migrate, hence by virtue of a higher density, sulphide melt displaces silicate melt as it percolates downwards. Importantly, most of the sulphide melt is mobilized prior to complete re-crystallization of the silicate and chromite aggregate layer. The initial mobilization of sulphide melt is therefore enhanced by an increased permeability and the possible absence of silicate melt due to the slower progression of the melting reaction in the silicates. Hence sulphide melt initially drains through interstitial gaps. At a temperature of 900 ^{O}C, only 100^{O}C above the likely sulphide solidus (~800^{O}C, Theron et al, 2011), aborted experiments, due to thermocouple failure, with ultra short runtimes (<5min) show that draining sulphide melt will reach the bottom of the charge within several minutes (flow rate, 1mm per min). However the speed of percolation, at >1000^{o}C, is considerably slower at 0.2mm per day.

In chromitite layers, chromite crystals reveal textures indicative of chemical reaction with the sulphide melt. Figure 7a illustrates a typical reaction rim between sulphide melt and chromite, similar textures characterise all short duration (24h) experiments between 950^{O}C and 1050^{O}C. Reaction rims are not observed in the longer 96h experiments and this is interpreted to be the result of re-crystallizing chromite crystals, destroying the original reaction textures. X-ray maps in figure 7b reveal that the chromite at the interface with the reaction texture has a

lower concentration of Fe than the starting chromite. In contrast, Cr concentrations appear un-affected at the sulphide melt - chromite interface. Additionally, during 96h experiments, Pt alloys can be seen as isolated nodules trapped by re-crystallized chromite minerals (figure 7c). Importantly, because chromites re-crystallize before quench, trapped Pt alloy nodules are not quench related, and were precipitated from the sulphide melt during the course of the experiment. Subsequently, these experiments demonstrate that Pt nodules may be physically removed from the sulphide magma by re-crystallising chromite crystals.

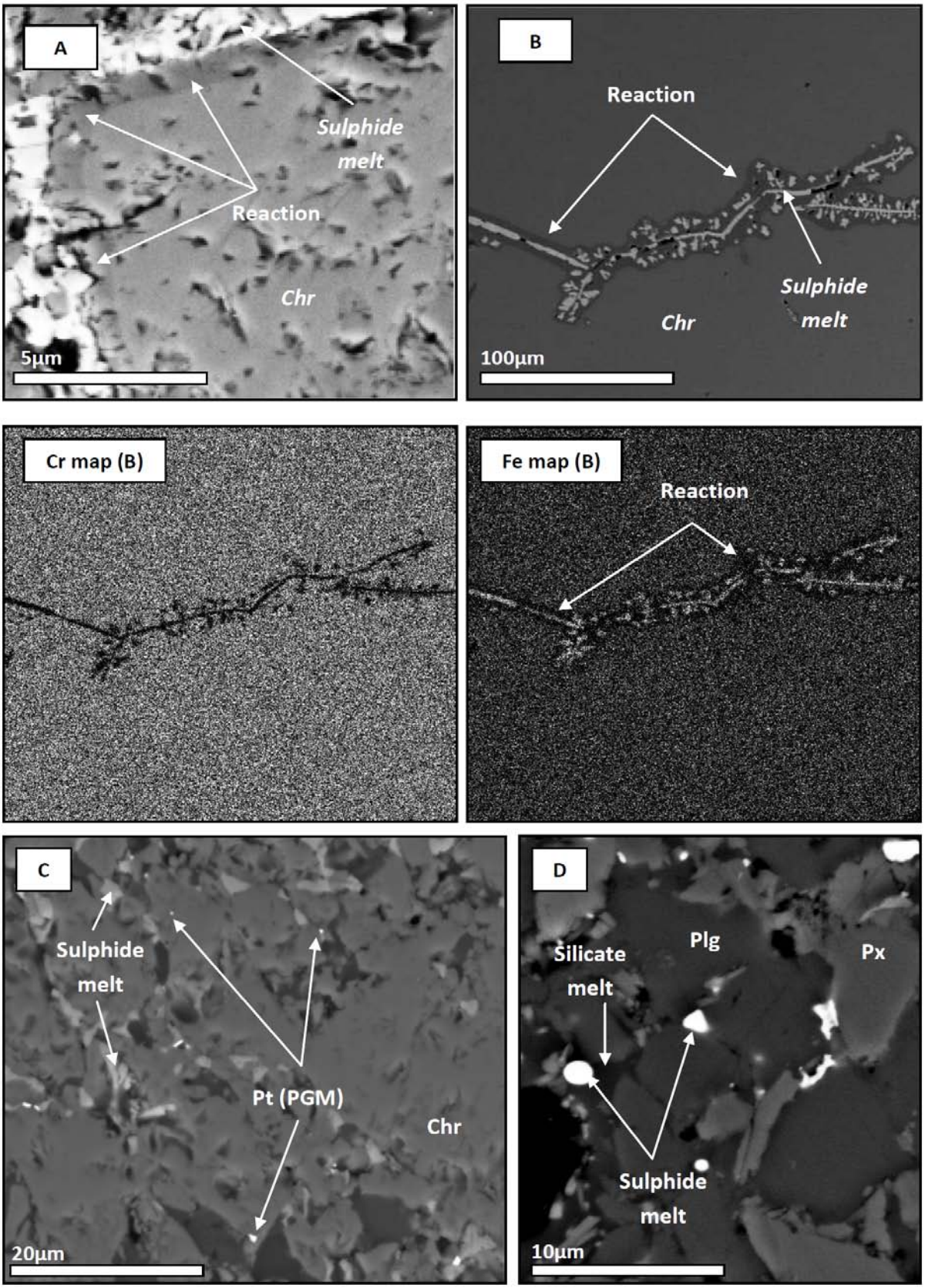

Figure 7: A) Chromites at 1000^{O}C (4kbar), during short experiments (24h) have not re-crystallized and are still relatively angular. Also visible are sulphide melts reacting with chromite creating reaction borders. **B)** Sulphide melt penetrating a fractured chromite grain in

a 1atm experiment at 1050^{O}C provides a clearer view of a reaction rim between sulphide melt and chromite. X-ray maps of Fe and Cr indicates that the chromite rims are partially depleted of Fe, however in contrast, Cr concentrations remain un-affected. **C)** In longer 96h experiments at 1000^{O}C (4kbar), chromite minerals are partially to completely re-crystallized, subsequently sulphide melt is forced into isolated round melt pockets, destroying melt networks. Pt (PGM) nodules can also be observed either at the chromite-sulphide melt interface or as isolated nodules trapped as inclusions between re-crystallizing chromite minerals. **D)** At 1050^{O}C Silicate and sulphide melt can be seen interstitially between re-crystallized minerals of pyroxene and plagioclase. Sulphide melt is completely wetted by silicate melt and is suspended as isolated droplets.

Sulphide compositions: Experiments at 1atm contain a sufficient volume of sulphide melt to accurately distinguish between sulphide melt and Mss. The analysis of Fe, Ni, Cu and S is possible without contamination from silicate and chromite minerals. Point EDS analysis was mainly used to analyze large homogeneous Mss crystals, while sulphide melt pools were analyzed by area quantitative EDS, due these being heterogeneous as a result of quench crystallization of the melt. Sulphide phase compositions from the chromite dominated (buffered) experiments at 1000^{O}C and 1150^{O}C and sulphide phases from the experiments without chromite (850^{O}C to 1050^{O}C), are presented in table 1a and 1b. In the chromite dominated experiments the liquidus is at least 100^{O}C (~1150^{O}C) higher than the liquidus (~1050^{O}C) observed in normal pure sulphide experiments. This indicates that the sulphide melts in these particular experiments are more Fe-rich and crystallize Mss at considerably higher temperatures. At 1000^{O}C sulphide melts, in comparison with pure sulphide experiments have lower Fe and S, and higher Ni and Cu.

In the 4kbar layered experiments, the interstitial sulphide phases in silicate and chromitite layers are too small and the quench crystallization products of melt, too coarse (due to quenching being much slower compared to 1atm), to confidently distinguish between MSS that existed at high temperature and that arising from quench crystallization of the melt. Therefore it is only possible to use area quantitative analysis by EDS to measure the bulk composition of the interstitial sulphide assemblage. The small areas scanned with relatively large volumes of sulphides range from 10µm – 100µm. The average of the scanned areas of a particular layer is regarded as the bulk composition for the sulphide assemblage in that particular layer.

Figure 8 illustrates a typical cross section of a layered 4kbar experimental run product and reveals firstly: Mss, which resides in-situ at the top of the charge and which coexisted with sulphide melt before it percolated away and secondly, how S, Fe, Ni and Cu are distributed by the segregation of Mss and melt during partial melting of the starting sulphide material and migration of the melt downwards in the capsule. Unlike in 1atm experiments, sulphides are located interstitially between minerals of pyroxene, feldspar and chromite, thus when analyzed by area quantitative EDS, sulphide compositions

are prone to contamination. Fe is present in multiple phases, including pyroxene, chromite and sulphides, while concentrations of S, Cu and Ni are negligible (<0.01 wt%) in pyroxene, feldspar and chromite. In this study we assume all of the Ni, Cu and S in the sample to be contained within the sulphide assemblage (an incorrect, but not unreasonable assumption). Consequently S, Ni and Cu compositions (normalised atomic %) are useful in predicting the presence and compositional variation of sulphide melt. In contrast, Mss crystals situated at the top of the layered charge were analysable without contamination.

Compositions for assemblages in silicate and chromitite layers produced in 4kbar experiments of $950^{O}C$ and $1000^{O}C$, together with relevant Mss compositions, are presented in table 2. Interstitial sulphide assemblages at $950^{O}C$ and $1000^{O}C$ in upper silicate layers have Ni/S ratios of 0.6 and 2.11, which are similar to 1atm sulphide melt Ni/S. In comparison Ni/Cu ratios of Mss are 5.93 and 7.33 respectively. In chromitite and lower silicate layers S, Ni and Cu show systematic variations in both $950^{O}C$ and $1000^{O}C$, which are described in the discussion regarding chromite interaction with sulphide melt.

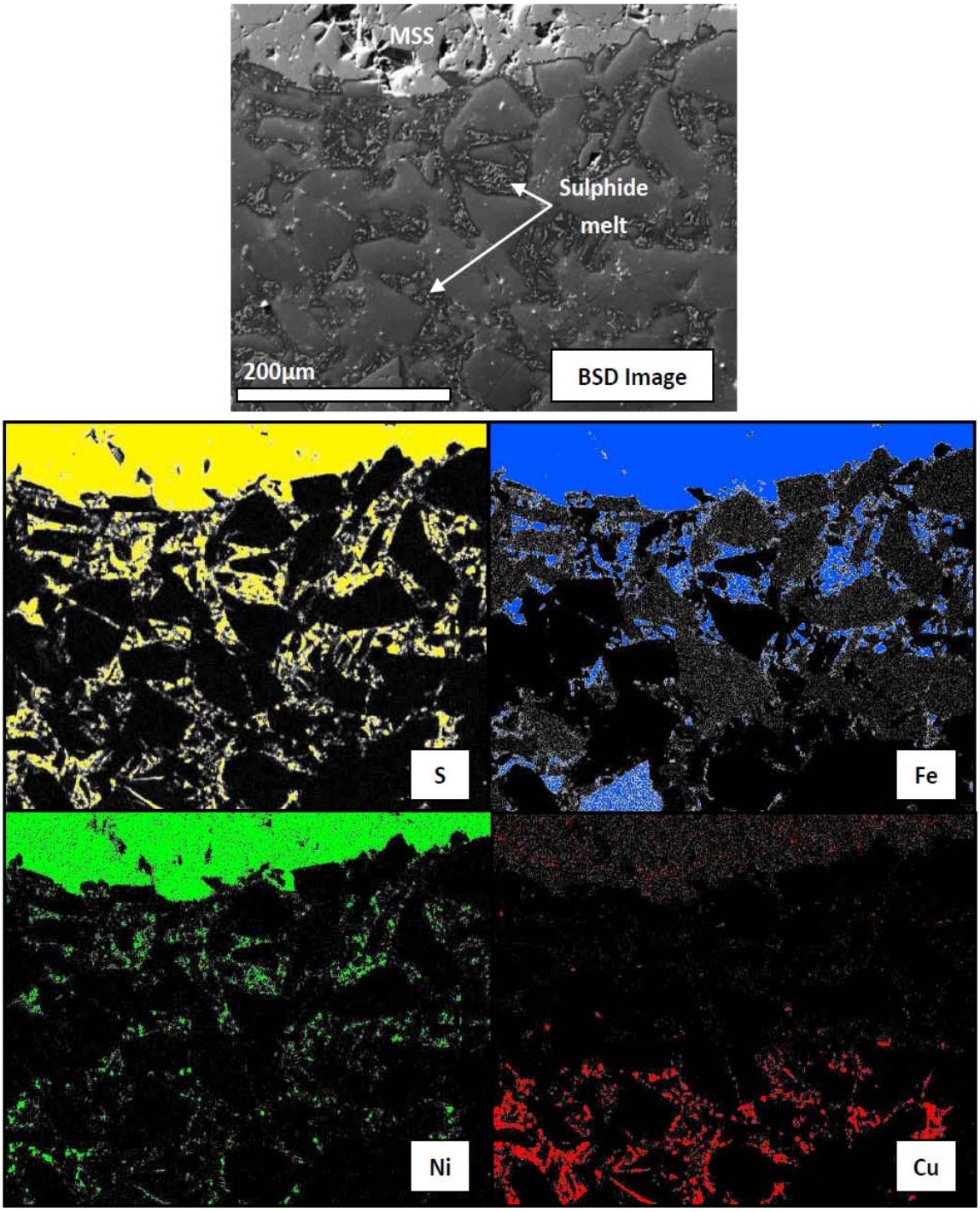

Figure 8: A BSD image and associated X-ray elemental maps of S (yellow), Fe (blue), Ni (green) and Cu (red) illustrates typical compositional trends of sulphide at multiple temperatures at 4kbar. This particular experiment was run at 950^{O}C for 30min, where after the temperature was increased to 1020^{O}C for 96h. MSS resides in-situ at the top of the upper silicate layer, while sulphide melt percolates away. At 950^{O}C a sulphide melt relatively enriched with Cu is produced and subsequently percolates down the entire charge. At 1020^{O}C the new sulphide melt produced is more Fe and Ni rich, which percolates and "overprints" the initial Cu rich sulphide melt for the first 1mm of the charge below the Mss (best illustrated by the Cu map).

Table 1a: Sulphide phase compositions in chromite dominated experiments (1atm)

Temp(^{O}C)	At%	S	Fe	Ni	Cu	metal/S
1150	Melt	47.46 ± 0.47	37.26 ± 0.43	10.98 ± 0.52	4.55 ± 0.94	1.11 ± 0.03
	Mss	50.59 ± 0.16	41.62 ± 0.39	5.61 ± 0.36	1.18 ± 0.12	0.95 ± 0.05
1000	Melt	47.14 ± 0.20	26.47 ± 0.28	18.64 ± 1.39	7.54 ± 1.39	1.11 ± 0.02
	Mss	50.92 ± 0.19	38.78 ± 0.54	8.05 ± 0.39	2.25 ± 0.29	0.96 ± 0.02

Table 1b: Sulphide Phase compositions (1atm)

1050	Melt	49.89 ± 0.07	33.54 ± 0.12	12.56 ± 0.06	5.41 ± 0.10	1.03 ± 0.002
	Mss	51.98 ± 0.29	41.18 ± 0.68	5.61 ± 0.69	1.28 ± 0.28	0.93 ± 0.01
1000	Melt	49.46 ± 0.05	33.32 ± 0.17	12.58 ± 0.26	5.67 ± 0.44	1.04 ± 0.003
	Mss	51.25 ± 0.14	40.34 ± 0.27	6.55 ± 0.24	1.86 ± 0.19	0.95 ± 0.004
950	Melt	48.72 ± 0.16	26.04 ± 0.30	15.80 ± 0.70	9.96 ± 0.41	1.04 ± 0.002
	Mss	50.51 ± 0.17	39.66 ± 0.21	7.95 ± 0.14	1.88 ± 0.14	0.97 ± 0.004
900	Melt	47.13 ± 0.06	27.62 ± 0.21	16.62 ± 0.38	10.21 ± 0.24	1.15 ± 0.005
	Mss	50.88 ± 0.15	39.67 ± 0.21	7.43 ± 0.18	2.02 ± 0.20	0.96 ± 0.003
850	Melt	45.74 ± 0.10	26.24 ± 0.34	14.40 ± 0.43	13.61 ± 0.42	1.19 ± 0.005
	Mss	50.64 ± 0.33	38.67 ± 0.56	8.79 ± 0.36	1.80 ± 0.60	0.97 ± 0.003

Table 2: Sulphide Phase compositions at (4Kbar)

Temp (^{O}C)	At%	S	Fe	Ni	Cu	Ni/Cu	Ni/S	Cu/S	metal/S
1000	Mss	51.37 ± 0.35	40.38 ± 0.35	7.23 ± 0.16	1.02 ± 0.16	7.33 ± 1.12	0.14 ± 0.003	0.02 ± 0.003	0.94 ± 0.08
	*Bulk Sulphide in upper Silicate	58.89 ± 1.58	n.a.	27.21 ± 1.79	13.89 ± 2.92	2.11 ± 0.61	0.46 ± 0.03	0.24 ± 0.014	n.a.
	*Bulk Sulphide melt in Chromitite	61.38 ± 1.66	n.a.	25.92 ± 1.65	12.70 ± 0.52	2.30 ± 0.15	0.42 ± 0.01	0.21 ± 0.012	n.a.
	*Highly evolved sulphide melt	57.57 ± 1.35	n.a.	25.84 ± 0.71	16.58 ± 0.64	1.56 ± 0.05	0.44 ± 0.02	0.28 ± 0.02	n.a.
950	Mss	50.61 ± 0.24	39.45 ± 0.37	8.32 ± 0.29	1.61 ± 0.13	5.19 ± 0.31	0.16 ± 0.06	0.03 ± 0.03	0.97 ± 0.05
	*Bulk Sulphide in upper Silicate	56.18 ± 2.39	n.a.	16.25 ± 2.04	27.06 ± 1.99	0.60 ± 0.10	0.28 ± 0.01	0.48 ± 0.05	n.a.
	*Bulk Sulphide in Chromitite	60.56 ± 1.18	n.a.	15.76 ± 0.83	23.67 ± 1.46	0.70 ± 0.06	0.26 ± 0.02	0.39 ± 0.03	n.a.
	*Highly evolved sulphide melt	54.04 ± 2.04	n.a.	13.45 ± 0.57	32.51 ± 1.73	0.41 ± 0.02	0.25 ± 0.02	0.60 ± 0.05	n.a.

Chromite compositions: Chromite mineral compositions and reaction rims for 4kbar experiments were analysed by point EDS and average compositions are listed in Table 3. Chromites are characterised by 3 different compositions: firstly, the original starting chromite composition; chromite rims that have undergone reaction with sulphide melt in the short duration experiments; thirdly, chromite that has partially to completely re-crystallised in longer duration experiments. Reaction rims with sulphide melt are not visible on the re-crystallized chromite crystals and these have re-crystallised, to an intermediate composition between that of starting chromite and reactions rims. Consequently, the reaction rims in the short duration runs should be regarded as a transient and disequilibrium phenomena. Cr and Ti concentrations in chromite are relatively constant and do not appear to be affected by interaction with sulphide melt (figure 9a, b), however Fe^{2+} and Fe^{3+} decreases severely in chromite at the sulphide melt interface (figure 9e, d). This is coupled by an increase of Mg^{2+} and Al^{3+} (figure 9c), consequently substituting for the loss of Fe^{2+} and Fe^{3+} respectively. Apart from sulphide melt preferentially leaching Fe^{2+} from chromite rims, the loss of Fe^{3+} is caused by conversion of Fe^{3+} to fe^{2+} through redox reactions involving graphite from the pressure cell. Note that the degree of the reaction between sulphide and chromite is enhanced by the large volume of sulphide melt (>5 volume %) in our experiments. In comparison the Merensky reef, considered to be the most sulphide rich of the reefs, the volume of sulphides in chromitite only account for up to 1.5% volume of the whole rock (Godel et al, 2007). Hence the reaction would not be as severe in the natural rocks.

Table 3: Average chromite mineral compositions

Wt%	Starting chromite	Re-crystallized chromite	Chromite rim in contact with sulp. melt
TiO_2	0.66 ± 0.07	0.73 ± 0.06	0.76 ± 0.08
Al_2O_3	18.71 ± 0.65	19.72 ± 0.34	22.85 ± 0.37
Cr_2O_3	44.02 ± 0.79	44.71 ± 0.95	46.95 ± 0.56
FeO	26.61 ± 0.32	23.59 ± 1.51	16.79 ± 1.04
MgO	9.52 ± 0.39	10.76 ± 0.37	12.09 ± 0.61
V_2O_5	0.48 ± 0.04	0.50 ± 0.03	0.56 ± 0.06
Cations on basis of 32 oxygen's			
Al	5.62 ± 0.17	5.86 ± 0.09	6.66 ± 0.11
Ti	0.13 ± 0.01	0.14 ± 0.01	0.14 ± 0.02
Cr	8.88 ± 0.21	8.91 ± 0.19	9.19 ± 0.10
Fe^{3+}	0.99 ± 0.07	0.70 ± 0.24	0.00 ± 0.00
Fe^{2+}	4.70 ± 0.13	4.28 ± 0.11	3.47 ± 0.23
Mg	3.62 ± 0.13	4.04 ± 0.12	4.46 ± 0.21
V	0.08 ± 0.01	0.08 ± 0.00	0.09 ± 0.01
Mg#	0.43 ± 0.02	0.49 ± 0.01	0.56 ± 0.03
Al/R3	0.36 ± 0.01	0.38 ± 0.01	0.42 ± 0.00
Cr/R3	0.57 ± 0.01	0.57 ± 0.01	0.57 ± 0.00
Ti/R3	0.008 ± 0.001	0.009 ± 0.001	0.009 ± 0.001
Fe3/R3	0.063 ± 0.004	0.045 ± 0.015	0.000 ± 0.000
	(n=27)	(n=10)	(n=16)

Mg# = Mg2+ / (Fe^{2+} + Mg^{2+}); R3 = (Al + Ti + Cr + Fe^{3+})

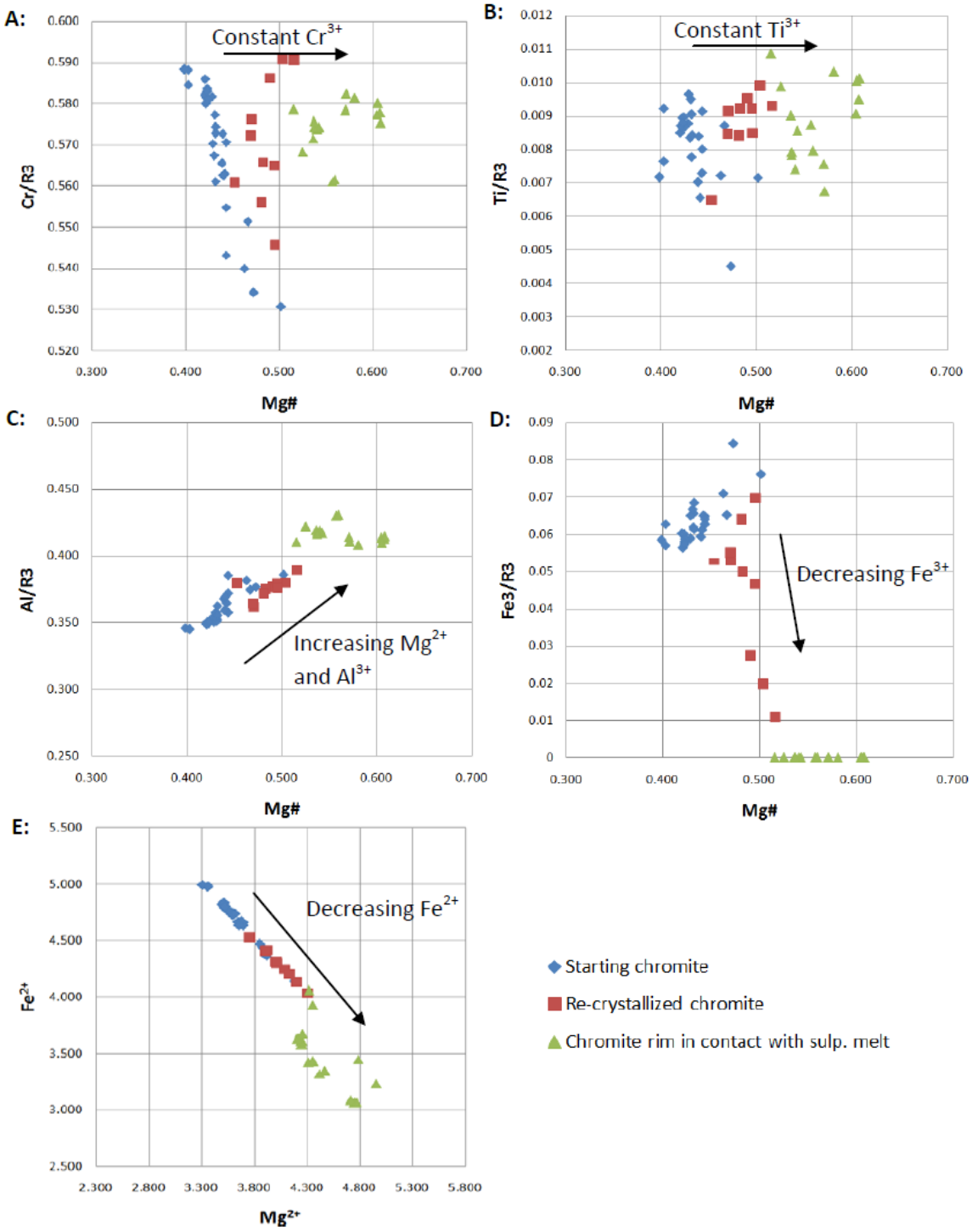

Figure 9: Plots of compositional variation between starting chromite, re-crystallized chromite and chromite rims that have interacted with sulphide melt. M# = Mg^{2+}/ (Fe^{2+}+Mg^{2+}); R3 = (Al^{3+}+Cr^{3+}+Ti^{3+}+Fe^{3+}).

Dihedral angle measurements: In this study, measurements were performed on randomly orientated 2-D sections observed via the SEM BSD. Dihedral angles in rocks vary due to anisotropy, however the median of the population of dihedral angles measured is close to the true, 3-D, dihedral angle (Harker & Parker, 1945; Riegger & Van Vlack, 1960). In experiments such as these, the isostatic nature of the stress field associated with pressure generation should not produce any anisotropy in the charge. Dihedral angles were measured with a standard angle measurement tool with the SEM on BSE images. Measurements are limited to 4kbar layered experiments with chromite-melt and silicate-melt representing chromitite and melanorite layers respectively. Measurements of sulphide melt between interfaces of pyroxene-pyroxene, plagioclase-plagioclase and plagioclase-pyroxene are combined for the silicate layer. In chromitite layers measurements involve only sulphide melt between chromite crystals. Results are listed in Table 4. In our experiments the median dihedral angle for sulphide melt-silicate is 33^{O} and for sulphide melt-chromite 11^{O}. Thus for relevant lihologies, including silicate (melanorite) and chromite (chromitite) the dihedral angle is significantly less than the $<60^{O}$ percolation threshold.

Table 4: Dihedral angle measurements

Temperature	Minerals-Sulphide melt	Median^{O}	Max^{O}	Min^{O}	n=
950^{O}C	chromite-melt	8	24	1	36
	silicate-melt	34	45	5	28
1000^{O}C	chromite-melt	15	31	1	18
	silicate-melt	29	35	19	9
1020^{O}C	chromite-melt	9	24	1	8
	silicate-melt	39	49	18	5
1050^{O}C	chromite-melt	10	24	1	6
	silicate-melt	31	33	19	3
Experimental Avg.	chromite-melt	11	26	1	68
	silicate-melt	33	41	15	45
Godel et al, 2006	chromite-melt	95	144	25	141
	silicate-melt	53	139	18	103

Discussion

In light of our results, the concentration of Pt by immiscible sulphide melts in chromitite reefs needs to consider the following: firstly, how sulphide melts mobilize through silicate and chromite cumulate horizons and if this behaviour coincides with temperatures that would cause fractionation of Pt between Mss and sulphide melt. Secondly, the implications of chemical interaction between sulphide melts and chromite minerals. Thirdly, how the behaviour of sulphide melt mentioned above will combine to contribute to Pt mineralization and extreme Pt/S associated with chromitites.

Sulphide melt mobility: Figure 10 illustrates the contrasting behaviour of sulphide melt topology in chromitite and silicate layers respectively. In contrast, dihedral angles measured by Godel et al, 2006, are much higher than experimental angles (95^{O} and 53^{O} for silicate- and chromite-melt respectively compared to experimental angles, 33^{O} and 11^{O}). Their measurements were however performed on natural rocks and considered the angles between sulphide minerals, typically pyrrhotite, chalcopyrite and pentlandite, and relevant silicate minerals and chromite of the Merensky reef. These minerals have undergone re-crystallization at sub-solidus temperatures, as evidenced by the fact that the sulphide minerals did not exist within the magmatic environment. Thus, the extent to which these measurements reflect the true dihedral angles between sulphide melt and the minerals through which sulphide melts percolated is uncertain. In contrast, in our experiments the original melt mineral texture is preserved through fast quenching, consequently preserving the true dihedral angle.

Sulphide melt was present in all experiments, whereas silicate melt was only present above 1000^{O}C (4kbar). Hence, at temperatures $<1000^{o}$C the solid silicate/chromite cumulate matrix would be impermeable due to the absence of silicate melt. A low dihedral angle (33^{O}) indicates that sulphide melt in the hanging wall silicate layers would have been able to percolate. In contrast, dihedral angles in the chromitite are extremely low (11^{O}), despite excellent interconnectivity, vertical percolation of small volumes sulphide liquid in the chromitite layer will be limited due to inter-granular capillary forces. As a result, and illustrated by figure 8, chromitite has a tendency to absorb sulphide liquid in a manner similar to a sponge absorbing water.

Considering temperatures just above 1000^{O}C, and a D_{pt} of 0.013 between sulphide melt and Mss, sulphide melt would have accounted for roughly 35% of the total volume of the sulphide system and contained the bulk of the Pt (Theron et al, in preparation). Thus the remaining 65% of the relatively Pt poor sulphide will reside in situ in the hanging wall silicate layer as crystallized Mss, while sulphide melt percolates away. Consequently, the window for maximum sulphide melt mobility coincides with temperatures down to 1000^{O}C where sulphide melts are evolved and enriched with Pt. However it seems likely that chromitites acted as a reservoir for evolved Pt, Ni and Cu rich sulphide melts percolating from hanging wall silicate layers. These findings are supported by many natural rock studies which highlight extreme spikes of Cu, Ni

and Pt concentration in chromitite layers relative to hanging wall anorthosite and melanorite layers in the Bushveld reefs (Cawthorn 1999 & 1999a, Godel et al. 2006 & 2007, Naldrett et al. 2009 & 2009b, Campbell & Naldrett 1979, Naldrett and Von Gruenewaldt 1989 and Brugmann et al. 1993).

However, formation temperatures of the Merensky reef are problematic. It was shown by Cawthorn and Davies, 1983, and later confirmed by Li et al, 2001, that the Merensky formed at 1180^{o}C. This very close to the thermal stability of pure Fe-S Mss (1190^{o}C), and considering that Ni and Cu will further lower its thermal stability, it is unlikely that fractionation occurred due to the crystallization of Mss. In contrast, Theron et al, in preparation, show that sulphide assemblages in the Merensky reef do resemble bulk sulphide compositions relating to fractionation. How, when and at what temperature immiscible sulphide formed remains a stumbling block for mineralization models in general and needs further investigation.

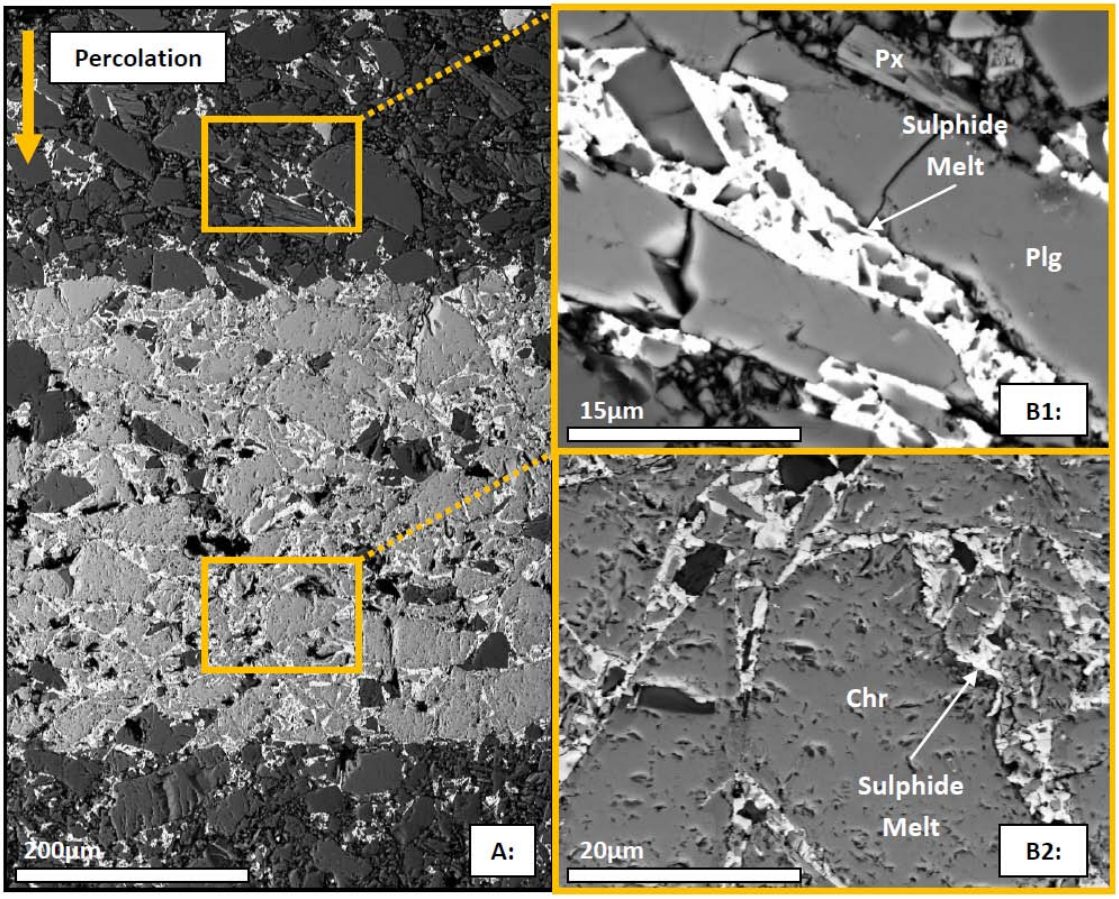

Figure 10: SEM BSD images of layered charge at 4Kbar, 1000^{O}C (24h). The large section shows percolated sulphide melt (very light grey) distribution in silicate (dark grey) and chromitite layers (intermediate grey). The two zoomed in images highlight the contrast between wetting properties of sulphide melt with respect to chromite and silicate minerals. Note the chromitite layer is completely saturated with sulphide melt, as all the grain

boundaries are wet. As a consequence excess sulphide melt escapes at the bottom of the layer.

***Sulphide melt – chromite interaction*:** Sulphide melt preferentially leaches Fe^{2+} from chromite rims, shifting chromite towards the spinel end-member. The effect of additional Fe^{2+} in the sulphide system can be observed in both 1atm and 4kbar layered experiments. Sulphide melts in a chromite dominated environment at $1000^{O}C$ (1atm) have higher atomic metal/S (1.11) compared to sulphide melts analysed in experiments with no chromite (1.04). Thus, the chemistry of the sulphide magma is changed by interaction with chromite. Additional Fe^{2+} leached from chromite, causes sulphide melt to crystallize extra Mss lowering its S content and increasing Ni and Cu concentrations. The effect of additional Fe^{2+} is also observed at $1150^{O}C$ where sulphide melt crystallizes Mss at least $75^{O}C$ above the expected liquidus of $1075^{O}C$ for the starting sulphide system (Theron et al, in preparation). In 4kbar layered experiments the average S concentrations of sulphide assemblages in chromitite layers increase by 3% between $1000^{O}C$ and $950^{O}C$ compared to sulphide assemblages located in the upper silicate (hanging wall). Consequently, Ni/S and Cu/S ratios decrease by 4% and 8% respectively. In contrast, silicates just below chromitites (footwall) contain sulphide assemblages with Cu/S ratios 9.5% higher than sulphide assemblages located in silicate above chromites. This indicates that sulphide melts entering the chromitite layer have crystallized Mss and that some of the evolved Cu rich melt have percolated away into the lower footwall. These observations are supported by 1atm experimental studies from Kullerud et al, 1969, which indicate that increasing the Fe/S ratio of sulphide melt, will raise the solidus temperate and at any given temperature below the liquidus and increase the amount of Mss crystallized.

The leaching of Fe^{2+} from chromites at a constant temperature is likely to be buffered by the effective concentration of S in sulphide melt. To determine the S saturated state in sulphide melt is difficult and varies according to composition and temperature. In pure sulphide experiments at $950^{O}C$ and $1000^{O}C$ the atomic metal/S ratios of sulphide melts coexisting with Mss are 1.04. However, for experiments with volumetrically dominant chromite metal/S at $1000^{O}C$ is 1.11. Thus sulphide melts in our experiments has sufficient S and are able to crystallize additional Mss down to at least $950^{O}C$ if the Fe^{2+} concentration is increased.

Considering the reaction process described above and that chromitite reefs were a likely reservoir for sulphide melt, chromite minerals in the reefs should arguably have lower Fe^{2+} concentrations relative to chromites in the hanging wall. Makwela, 2011, analysed natural chromite minerals of the Merensky reef according to litho-stratigraphy which included, normal Merensky (pyroxenite, melanorite), upper and lower chromitites. Chromites located in the lower chromitite have 2.3 wt% lower FeO compared to the chromites in the normal Merensky located directly above (hanging wall). Similarly, chromites in the upper chromitite layer are lower by 4.44 wt% FeO. This indicates that

chromites likely lost Fe^{2+} to sulphide melts.

Crystallization of Platinum Alloys: Chromitites in layered experiments with long run times (96h) contain Pt alloy nodules roughly 1µm in diameter. Pt nodules within chromitite layers are associated with extremely small amounts of sulphide melt, to the extent that it is highly unlikely the Pt alloy quench crystallised from the sulphide melt represented by the associated sulphide. In the most extreme cases, Pt nodules are completely isolated, in the 2 dimensional view available, (figure 6B) and decoupled from sulphide. Consequently, such Pt alloy nodules cannot be the result of quench crystallization and must have formed whilst the experiment was equilibrating under normal run conditions. We argue that Pt alloys precipitate/crystallize when sulphide melt is still mobile and whilst chromite crystals are re-crystallising. Hence sulphide melt is able to move away from precipitated Pt nodules. Considering that the initial volume of sulphide melt is low and a very effective wetting medium for chromite, most of the interstitial sulphide melt will be retained in the chromitite layer. The isolation of crystallised Pt nodules will predominantly be caused by the re-crystallization of chromite minerals, subsequently squeezing away the sulphide melt from which the Pt alloy crystallised. In contrast, Pt nodules in silicate layers bear no resemblance to nodules observed in chromitites. These Pt nodules are only observed within large melt pools, arguably forming during quenching of the sulphide melt.

Pt alloy distribution in chromitites suggests that Pt rich sulphide melt in chromitites become oversaturated with Pt, resulting in the formation of Pt alloys. Peregoedova et al, 2004 states that by decreasing the S-content of sulphide melt sufficiently, it is possible to precipitate Pt alloys. We argue that S saturated sulphide melt containing dissolved Pt interacts with chromite (as previously discussed). Consequently sulphide melt is forced to crystallize additional Mss, hence the residual Cu-Ni-S melt loses S, lowering Pt solubility and forcing Pt to crystallise as alloys. Consequently chromitites acts as a Pt filter for percolating Pt-bearing sulphide melt.

This this interpretation is limited, due Pt being the sole PGE and as a result formed only Pt alloys. To estimate how much this process contributed to initial Pt mineralization is difficult. A variety of PGM could have formed under S saturated Merensky magmatic conditions, and how these alloys might have been affected by late re-crystallization processes in the Merensky we do not know. Currently in Merensky reef chromitite layers, only 0.2% to ~12% of PGE is present in BMS (base metal sulphides), hence the bulk of PGE exists as discrete PGM phases (Godel et al, 2007). It's impossible to determine how much of the current PGM assemblage was initially dissolved in higher temperature Mss/Iss (intermediate solid solid-solution) or how much PGM crystallised out of sulphide melt at temperatures >850^{o}C. However, Pt solubility of sulphide melt would have decreased when in contact with chromite and is likely to have contributed to the formation of discrete high temperature PGM phases. Further experiments could well examine what conditions suite the crystallization of relevant PGM and help to

distinguish between primary and secondary Pt mineralization episodes.

Model for Bushveld Pt Mineralization

We propose a revised model for Pt mineralisation that is similar to the model proposed by Godel et al, 2006, 2007, but importantly, is grounded in our experimental findings. In light of the experimental evidence, the primary mechanism for Pt enrichment in the chromitites is the infiltration of a Pt-bearing sulphide melt. Contrasting wetting properties of sulphide melt in contact with chromite and the minerals of the melanorite layers, as well as leaching of Fe^{2+} from chromite by sulphide melt, are important secondary mechanisms that control mineralization.

Mineralization model: This model assumes the hypothesis that the formation of immiscible sulphide was synchronous with the accumulation of silicate minerals in mineralized reef horizons (Cawthorn, 1999[b]). Downwards percolating immiscible sulphide melt in the silicate hanging wall above chromitite layers crystallizes Fe rich Mss (up to 65 volume%; Theron et al, in preparation) in situ. As a result, the evolved sulphide melt reaching chromitite layers has a lower volume than the parental sulphide melt. Evolved sulphide melts will have much higher Pt concentrations due the combined effect of preferential partitioning of Pt into sulphide liquid (D_{Pt} = 0.013 at 1000^{O}C, Theron et al, in preparation) and a lower volume. An extremely low dihedral angle in chromitites will significantly increase melt retention of percolating sulphide melt within the chromitite layer due to strong capillary action, however volumes of trapped sulphide melt will be low due to decreasing permeability as chromite minerals anneal/coalesce. Thus chromitite layers act as a reservoir, trapping evolved Cu, Ni and Pt rich sulphide melt. The trapped sulphide melt will leach Fe^{2+} from chromite minerals, increasing the Fe concentration within sulphide melt. This forces sulphide melts to crystallize Mss, driving the sulphide melt towards a more Cu-rich and lower S composition. Decreasing S-content in sulphide melt decreases Pt solubility in the melt (Peregoedova et al, 2004), hence Pt alloys are precipitated. Concurrent re-crystallizing and coalescing of chromite minerals results in the physical separation of Pt alloy nodules from sulphide melt, explaining the fact that in the chromitite reefs (and in the experiments), Pt nodules can occur that are not in contact with sulphide. Sulphide melt draining out of the chromitite layer will be even lower in volume, Cu-rich and depleted in Pt when compared with the sulphide melt that entered the chromitite layer. A graphical illustration of these processes is provided in figure 11.

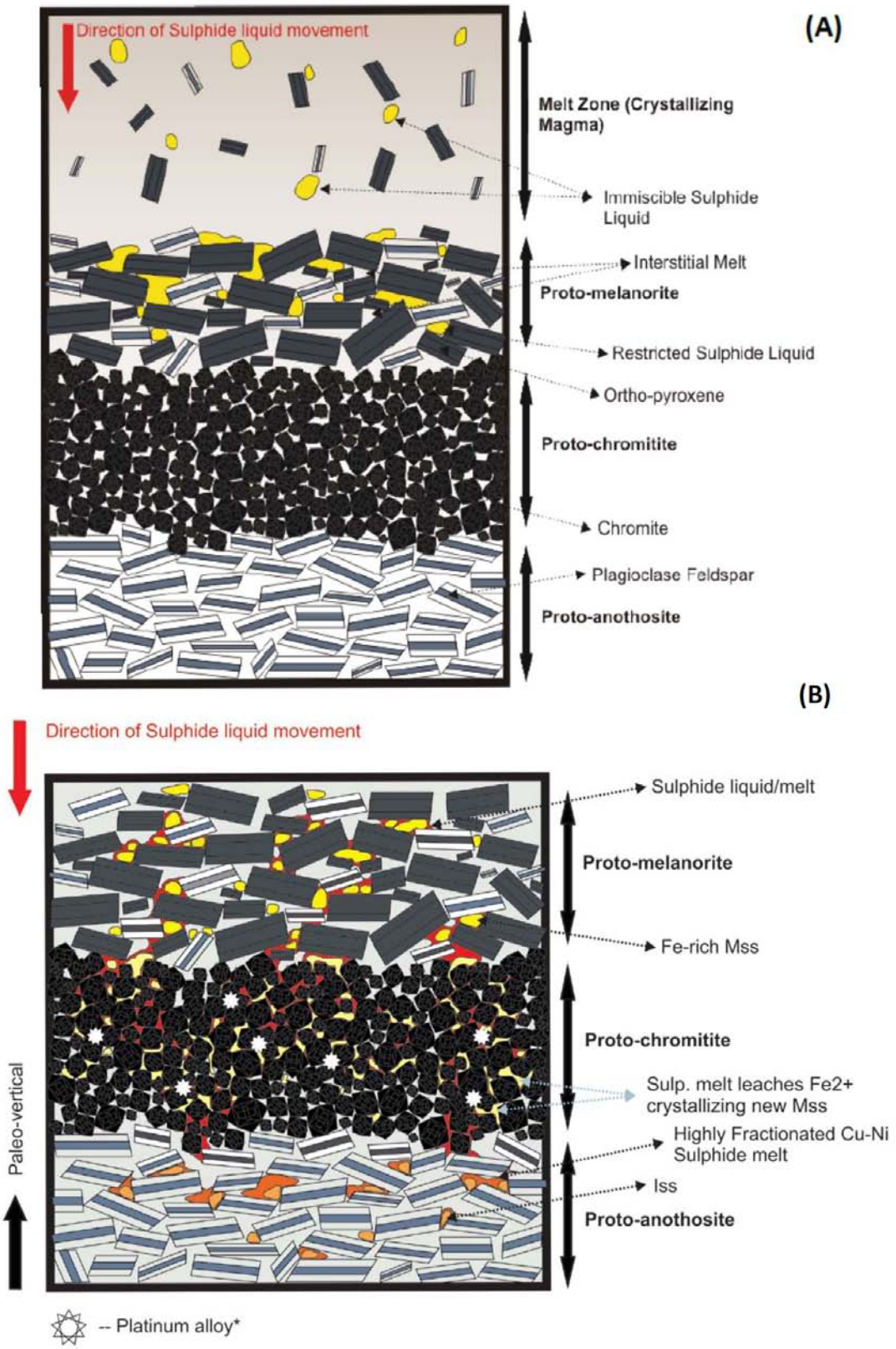

Figure 11: Model for Pt mineralization. **(A)** At high temperature (>1000^{O}C) the movement of a relatively un-fractionated sulphide melt is restricted by interstitial silicate melt. **(B)** During progressive cooling the volume of silicate melt decreases allowing sulphide melt to

percolate via melt networks. Fractionation occurs as Pt, Cu and Ni rich sulphide melt segregates from crystallizing Fe-rich MSS. The vertical percolation of sulphide melt is however stalled due to high melt retention in chromitites. The leaching of Fe^{2+} from chromite forces the crystallization of Mss and subsequently reduces the S-content of residual sulphide melt. This reduces the Pt solubility of sulphide melt resulting in the formation of Pt alloys. A small proportion of highly fractionated Cu-Ni-rich sulphide melt escapes through the bottom of the chromitite layer and crystallizes mostly Cu rich Iss.

Conclusion

There is a general consensus that immiscible sulphide is the primary concentrator of Pt in mineralized reefs of the Bushveld. In this study, we observed several processes that could contrubute how Pt is concentrated by sulphide liquid.

Experimental observations findings are as follows:

1) Experimental dihedral angles of chromite (11^o) and silicate (33^o) in contact with sulphide melt are significantly less than the percolation threshold (60^o). This shows that sulphide melt/liquid is an efficient wetting medium. The theory, based on relatively high dihedral angles (95^o) in chromitites, that chromitite layers acted as a barrier to downwards migrating sulphide liquid (Godel et al, 2006) is wrong.

2) Experimental chromite mineral properties indicate that chromitite layers is likely to have acted as a reservoir for evolved (fractionated) sulphide melts due to a higher melt retention capacity than surrounding silicate lithologies. However, compaction and re-crystallizing of chromite minerals would severely reduce the permeability of chromitite layers. Despite its high retention capabilities, chromitite layers would have had a limited and continuously decreasing interstitial space to retain sulphide melt. Thus it is likely that only a very small proportion of sulphide melt ever migrated into chromitite.

3) Notably, we could not find any evidence to support the popular theory that chromite re-equilibration lead to the destruction of interstitial sulphide via chromite scavenging Fe^{2+} from sulphide. In contrast, we find the opposite to be true. Sulphide reacting with chromite gains additional Fe^{2+} and crystallizes Mss, hence decreasing the S content of the sulphide melt and Pt solubility. Thus chromitite layers not only trap sulphide melt, but promote the formation of Pt alloys (PGM).

4) These processes could well explain the extreme Pt/S ratios observed in chromitites without the need for any prior formation of PGM before sulphide saturation.

Reference List

- Ballhaus, C. and Sylvester, P., 2000, Noble Metal enrichment Processes in the Merensky Reef, Bushveld Complex: Journal of Petrology, v.41(4), p.545-561
- Ballhaus, C., Bockrath, C., Wohlgemuth-Ueberwasser, C., Laurenz, V., Berndt, J., 2006, Fractionation of Nobal Metals by Physical Processes: Contrib Mineral Petrol, v.152, p.667-684
- Barnes, S.J. & Maier, W. D., 2002, Platinum-group elements and microstructures of Normal Merensky Reef from Impala Platinum Mines, Bushveld Complex: Journal of Petrology, v.43(1), p.103-128
- Barton, P.B. Jr., 1970, Sulphide petrology: Mineralogical Society of America Special Paper 3, p.187–198.
- Bezman, N.L., Azif, M., Brugman, G.F., Romanenko, L.M. and Naldrett, A.J., 1994, Distribution of Pd, Ir, Os and Au between sulphide and silicate melts: Geochim. Cosmochim. Acta., v.58, p.1251-1260
- Bockrath, C., Ballhaus, C., 2002, PGE fractionation between sulfide- bearing mantle and basaltic melt during partial melting and melt segregation: In Proceedings of the 9th international platinum symposium, abstract with program, 21–25, Billings, Montana, p.41–43
- Bockrath, C., Ballhaus, C., and Holzheid, A., 2004, Fractionation of the Platinum-Group Elements During Mantle Melting: Science, v. 305, p. 1951-1953.
- Brugmann, G. E., Naldrett, A. J., Asif M., Lightfoot, P. C., Gorbachev, N. S. & Fedorenko, V. A., 1993, Siderophile and chalcophile metals as tracers of the evolution of the SiberianTrap in the Noril'sk region, Russia: Geochimica et Cosmochimica Acta, v.57(9), p.2001-2018
- Bulau, J. R., Waff, H. S. & Tyburczy, J. A., 1979, Mechanical and thermodynamic constraints on fluid distribution in partial melts: Journal of Geophysical Research, v.84, p.6102–6108
- Campbell, I. H. & Naldrett, A. J., 1979, The influence of silicate silicate:sulphide ratios on the geochemistry of magmatic sulphides: Economic Geology, v.74, p.1503-1505
- Campbell, I. H., Naldrett, A. J. & Barnes, S. J., 1983, A model for the origin of the platinum-rich sulfide horizons in the Bushveld and Stillwater Complexes: Journal of Petrology, v.24, p.133-165
- Cawthorn, R.G. and Davies, G., 1983, Experimental Data at 3 Kbars Pressure on Parental Magma to the Bushveld Complex: Contrib Mineral Petrol, v.83, p.128-135
- Cawthorn, R.G., Lee, C.A., Schouwstra, R.P., Mellowship, P., 2002, Relationship between PGM and PGE in the Bushveld Complex: The Canadian Mineralogist, v.40, p.311-328
- Cawthorn, R. G., 2002, The role of magma mixing in the genesis of PGE mineralization in the Bushveld Complex, Thermodynamic calculations and new interpretations discussion: Economic Geology, v.97, p.663-667
- [a] Cawthorn, R.G., 1999, Permeability of the footwall cumulates of the Merensky Reef, Bushveld Complex: South African Journal of Geology, v.102(3), p.293-310

- [b] Cawthorn, R.G., 1999, Platinum-group element mineralization in the Bushveld Complex – a critical reassessment of geochemical models: South African Journal of Geology, v.102(3), p.268-281
- Coghill, B.M., and Wilson, F., 1998, Platinum group minerals in the Selukwe subchamber, Great Dike Zimbabwe – Implications for PGE collection mechanisms and post-formation redistribution: Mineralog Mag., v.57, p.613-633
- de Bremon d'Ars, J.D., Arndt, N.T., Hallot, E., 2001, Analog experimental insights into the formation of magmatic sulfide deposits: Earth Planet Sci Lett, v.186, p.371–381
- Eales, H. V., 2000, Implications of the chromium budget of the Western Limb of the Bushveld Complex: South African Journal of Geology, v.103, p.141 – 150
- Eales, H. V. and Cawthorn R.G., 1996, The Bushveld complex, Layered Intrusions: Elsevier Science B.V., p.181-229.
- Finnigan, C.S., Brenan, J.M., Mungall, J.E. and McDonough, W.F., 2008, Experiments and Models Bearing on the Role of Chromite as a Collector of Platinum Group Minerals by Local Reduction: Journal of Petrology, v.49(9), p.1647-1665
- Fleet, M.F., Crocket, J.H. and Stone, W.E., 1996, Partitioning of Platinum group elements (Os, Ir, Ru, Pd, Pt) and gold between sulphide liquid and basalt melt: Geochim. Chosmohim. Acta, v.60, p.2397-2412.
- Fleet, M.E. and Yuanming, P., 1994, Fractional crystallization of anhydrous sulfide liquid in the system Fe-Ni-Cu-S, with application to magmatic sulfide deposits: Geochim. Chosmohim. Acta, v.58(16), p.3369-3377
- Godel, B., Barnes, S.J. and Maier, W.D., 2006, 3-D Distrubution of Sulphide minerals in the Meresnsky reef (Bushveld Complex, Soputh-Africa) and The J-M reef (Stillwater Complex, USA) and their relationship to Microstructures using X-Ray tomography: Journal of petrology, v.47(9), p.1853-1872.
- Godel, B., Barnes, S.J. and Maier, W. D., 2007, Platinum-group elements in sulphide minerals, platinum-group minerals, and the whole rock of the Merensky Reef (Bushveld Complex, South Africa): Implication for the formation of the reef: Journal of Petrology, v.48, p.1569-1604
- Harker, D. & Parker, E. R., 1945, Grain shape and grain growth: Transactions of the American Society of Metals, v.34, p.156–195.
- Herring, C., 1951, Surface tension as a motivation for sintering. In: Kingston, W. E. (ed.): Physics of Powder Metallurgy, New York: McGraw–Hill, p.143–179.
- Holness, M. B., 2005, Melt-solid Dihedral Angles of Common Minerals in Natural Rocks: Journal of Petrology, v.47(4), p.791-800
- Kruger, F. J., 2005, Filling the Bushveld Complex magma chamber: lateral expansion, roof and floor interaction, magmatic unconformities, and the formation of giant chromitite, PGE and Ti-V-magnetitite deposits: Mineralium Deposita, v.40, p.451-472
- Kullerud, G., Yund, R. A., and MOH, G. H., 1969, Phase relations in the Cu-Fe-S, Cu-Ni-S and Fe-Ni-S systems: Econ Geology, v.4, p.323-343
- Kushiro, I., Yoder, H.S., Mysen, B.O., 1976, Viscosities of basalt and andesite melts at high pressures: J Geophys Res, v.81, p.6351– 6356
- Li, C., Barnes, S.J., Makovicky, E., Rose-Hansen, J., and Makovicky, M., 1995, Partitioning of nickel, copper, iridium, rhenium, platinum and

palladium between monosulfide solid solution and sulphide liquid: Effects of composition and temperature: Geochimica et Cosmochimica Acta, v.60(7), p.1234-1238

- Li, C. & Ripley, E. M., 2005, Empirical equations to predict the sulfur content of mafic magmas at sulfide saturation and applications to magmatic sulfide deposits: Mineralium Deposita, v.40, p.218-230
- Li, C., Maier, W. D. & de Waal, S. A., 2001, The role of magma mixing in the genesis of PGE mineralisation in the Bushveld Complex: Thermodynamic calculations and new interpretations: Economic Geology, v.96, p.653-662
- Lorand, J. P., Alard, O., Luguet, A. & Keays, R. R., 2003, Sulfur and selenium systematics of the subcontinental lithospheric mantle: inferences from the Massif Central xenolith suite (France): Geochimica et Cosmochimica Acta, v.67(21), p.4137-4151.
- Makwela, L., 2011, Examination of chromite compositions in the Bushveld Complex, with particular emphasis on the Merensky reef, Honours Thesis, University of Stellenbosch Department of Earth Science, p.1-56
- Merke, R.K.W., 1992, Platinum group minerals in the middle group of chromitite layers at Marikana, Western Bushveld Complex: Indications for collection mechanisms and post magmatic modification: Can. J. Earth Sci., v.29, p.209-221
- Minarik, W. G. & Watson, E. B., 1995, Interconnectivity of carbonate melt at low melt fraction: Earth and Planetary Science Letters, v.133, p.423–437
- Naldrett, A. J., 1989, Magmatic Sulfide Deposits: Oxford Mono. Geol. Geophys. No. 14. Clarendon.
- Naldrett, A.J. and Von Gruenewaldt, G., 1989, Assosiation with platinum group elements with chromitite in layered intrusions and ophiolite complexes: Economic Geology, v.84, p.180-187
- [a] Naldrett, A.J., Kinnaird, J., Wilson, A., YudovsKaya, M., McQuade S., Chunnet G. and Stanley C., 2009, Chromite composition and PGE content of the Bushveld chromitites: Part1 – The lower and middle groups: Applied Earth Science (Trans. Inst. Min. Metall. B), v.118(¾), p.131-161
- Naldrett, A.J. and Lehmann, J., 1988, Spinel non-stoichiometry as the explanation for Ni- Cu- and PGE-enriched sulphides in chromitites: *In* Geoplatinum '87 (eds. H. Prichard P. Potts J. Bowles and S. Cribb) Elsevier London, p.93-110
- [b] Naldrett, A. J., Wilson, A., Kinnaird, J. & Chunnett, G., 2009, PGE tenor and Metal Ratios within and below Merensky Reef, Bushveld Complex: Implications for its Genesis, Journal of Petrology, v.50(4), p.625-659
- Nell, J., 1984, Geochemical and thermodynamic controls on the formation of mineral assemblages from the metamorphic aureole of the Bushveld Complex in Potgietersrus Area: Msc thesis, University of Pretoria, Pretoria, South-Africa.
- Peregoedova, A., Barnes, S.J., Baker, D.R., 2004, The formation of Pt-Ir alloys and Cu-Pd rich sulphide melts by partial desulphurization of Fe-Ni-Cu sulphides: results of experiments and implications for natural systems: Chemical Geology, v.208, p.247-264
- Riegger, O. K. & Van Vlack, L. H. W., 1960, Dihedral angle measurement: Transactions of the Metallurgical Society of the AIME, v.218, p.933–935.
- Seabrook, C. L., Cawthorn, R. G. & Kruger, F. J., 2004, Geochemical disequilibrium in the Merensky and

Bastard Reefs, Eastern Bushveld Complex: Co-accumulation of minerals from stratified magmas: Economic Geology, v. 100, p. 1191-1206

- Smith, C. S., 1964, Some elementary principles of polycrystalline microstructure: Metallurgical Reviews, v.9, p.1–48
- Stevens, G., Prinz, S., Rozendaal, A., 2005, Partial melting of the assemblage sphalerite + galena + pyrrhotite + chalcopyrite + sulphur: Implications for high grade metamorphosed massive sulfide deposits: Economic Geology, v.100, p.781-786
- Theron, L.M., Koegelenberg, C. and Stevens, G., Phase relations in the Fe-Ni-Cu-S System at 1 atm: Implication for Evolution of Sulphide Fractionation in the Merensky reef, Western Bushveld Complex, South Africa: In preparation.
- Tredoux, M., Lindsy, N.M., Davies, G. and McDonald, I., 1995, The Fractionation of Platinum group elements in magmatic systems with the suggestion of a noval casual mechanism: South African Journal of Geology, v.58, p.157-167
- Wark, D. A. & Watson, E. B., 1998, Grain-scale permeabilities of texturally equilibrated, monomineralic rocks: Earth and Planetary Science Letters, v.164, p.591–605.
- Watson, E. B., 1982, Melt infiltration and magma evolution: Geology, v.10, p.236–240
- Wohlgemuth-Ueberwasser, C.C., Ballhaus, C., Barndt, J., ne´e Paliulionyte, V.S., Meisel, T., 2007, Synthesis of PGE Sulphide standards for Laser ablation inductively coupled mass spectrometry (LA-ICP-MS): Contrib mineral Petrol, v.154, p.607-617

3. Appendix

a. Starting chromite spectrum compositions

Wt%	Spectrum 1	Spectrum 2	Spectrum 3	Spectrum 4	Spectrum 5	Spectrum 6	Spectrum 7	Spectrum 8	Spectrum 9	Spectrum 10	Spectrum 11	Spectrum 12
TiO2	0.689	0.726	0.698	0.703	0.734	0.713	0.728	0.714	0.770	0.743	0.579	0.783
Al2O3	18.063	18.167	18.070	17.980	18.260	18.176	18.197	18.161	18.181	17.777	17.820	18.394
Cr2O3	44.854	44.752	44.977	45.013	44.218	44.955	44.873	44.979	44.550	45.090	45.151	44.062
FeO	26.817	26.748	26.570	26.582	26.869	26.420	26.582	26.516	26.617	27.193	27.373	26.946
MgO	9.128	9.180	9.209	9.178	9.444	9.319	9.212	9.195	9.423	8.731	8.602	9.376
V2O5	0.449	0.428	0.476	0.545	0.477	0.416	0.408	0.435	0.458	0.467	0.475	0.439
Cations on basis of 32 oxygens												
Al	5.459	5.486	5.458	5.435	5.501	5.483	5.493	5.484	5.480	5.394	5.410	5.540
Ti	0.133	0.140	0.135	0.136	0.141	0.137	0.140	0.138	0.148	0.144	0.112	0.150
Cr	9.093	9.065	9.113	9.127	8.936	9.098	9.087	9.111	9.008	9.178	9.196	8.903
Fe3+	0.940	0.938	0.904	0.878	1.023	0.920	0.919	0.896	0.968	0.890	0.914	1.016
Fe2+	4.824	4.807	4.803	4.835	4.737	4.749	4.788	4.798	4.740	4.977	4.996	4.759
Mg	3.489	3.506	3.519	3.509	3.599	3.556	3.518	3.512	3.593	3.351	3.304	3.573
V	0.076	0.073	0.081	0.092	0.080	0.070	0.069	0.074	0.077	0.079	0.081	0.074
Mg#	0.420	0.422	0.423	0.421	0.432	0.428	0.424	0.423	0.431	0.402	0.398	0.429
Al/R3	0.349	0.351	0.350	0.349	0.353	0.351	0.351	0.351	0.351	0.346	0.346	0.355
Cr/R3	0.582	0.580	0.584	0.586	0.573	0.582	0.581	0.583	0.577	0.588	0.588	0.570
Ti/R3	0.009	0.009	0.009	0.009	0.009	0.009	0.009	0.009	0.009	0.009	0.007	0.010
Fe3/R3	0.060	0.060	0.058	0.056	0.066	0.059	0.059	0.057	0.062	0.057	0.058	0.065
Re-calculated Wt% with Fe2O3												
TiO2	0.69	0.72	0.69	0.70	0.73	0.71	0.72	0.71	0.77	0.74	0.58	0.78
Al2O3	17.96	18.07	17.97	17.89	18.15	18.08	18.10	18.07	18.08	17.69	17.73	18.28
Cr2O3	44.61	44.51	44.74	44.78	43.95	44.71	44.63	44.74	44.30	44.86	44.91	43.80
Fe2O3	4.85	4.84	4.66	4.52	5.29	4.75	4.74	4.62	5.00	4.57	4.69	5.25
FeO	22.37	22.31	22.29	22.43	22.03	22.07	22.23	22.28	22.03	23.00	23.07	22.13
V2O5	0.35	0.33	0.37	0.42	0.37	0.32	0.32	0.34	0.36	0.36	0.37	0.34
MgO	9.08	9.13	9.16	9.13	9.39	9.27	9.16	9.15	9.37	8.69	8.56	9.32

Starting chromite spectrum compositions (continued)

Spectrum 13	Spectrum 14	Spectrum 15	Spectrum 16	Spectrum 17	Spectrum 18	Spectrum 19	Spectrum 20	Spectrum 21	Spectrum 22	Spectrum 23	Spectrum 24	Spectrum 25	Spectrum 26	Spectrum 27
0.680	0.615	0.655	0.574	0.594	0.593	0.599	0.634	0.684	0.744	0.682	0.717	0.594	0.374	0.537
18.567	17.724	19.420	19.166	20.430	18.932	20.168	18.859	18.399	18.587	18.630	19.674	20.044	19.888	19.303
43.921	44.763	43.139	43.906	41.899	43.548	42.369	43.494	44.267	44.233	44.239	43.150	42.264	42.012	43.794
26.988	27.605	26.532	26.231	25.400	26.580	26.560	27.093	26.605	26.273	26.233	25.744	26.362	26.856	26.259
9.402	8.746	9.752	9.611	11.181	9.734	9.771	9.449	9.480	9.713	9.649	10.288	10.230	10.416	9.635
0.443	0.548	0.502	0.514	0.495	0.614	0.532	0.471	0.565	0.450	0.567	0.427	0.506	0.454	0.472
5.587	5.377	5.810	5.747	6.026	5.677	6.015	5.666	5.539	5.582	5.598	5.859	5.961	5.908	5.783
0.131	0.119	0.125	0.110	0.112	0.113	0.114	0.122	0.131	0.143	0.131	0.136	0.113	0.071	0.103
8.866	9.111	8.658	8.831	8.291	8.760	8.476	8.766	8.940	8.911	8.916	8.619	8.431	8.372	8.802
1.044	0.979	1.013	0.930	1.190	1.011	0.999	1.068	0.957	0.979	0.924	1.019	1.109	1.324	0.957
4.736	4.979	4.636	4.665	4.149	4.660	4.637	4.725	4.741	4.635	4.682	4.437	4.473	4.365	4.639
3.579	3.357	3.691	3.645	4.172	3.692	3.686	3.591	3.610	3.690	3.667	3.875	3.848	3.914	3.652
0.075	0.093	0.084	0.086	0.082	0.103	0.089	0.079	0.095	0.076	0.096	0.071	0.084	0.076	0.079
0.430	0.403	0.443	0.439	0.501	0.442	0.443	0.432	0.432	0.443	0.439	0.466	0.462	0.473	0.440
0.358	0.345	0.372	0.368	0.386	0.365	0.385	0.363	0.356	0.357	0.360	0.375	0.382	0.377	0.370
0.567	0.585	0.555	0.565	0.531	0.563	0.543	0.561	0.574	0.571	0.573	0.551	0.540	0.534	0.563
0.008	0.008	0.008	0.007	0.007	0.007	0.007	0.008	0.008	0.009	0.008	0.009	0.007	0.005	0.007
0.067	0.063	0.065	0.060	0.076	0.065	0.064	0.068	0.061	0.063	0.059	0.065	0.071	0.084	0.061
0.68	0.61	0.65	0.57	0.59	0.59	0.60	0.63	0.68	0.74	0.68	0.71	0.59	0.37	0.53
18.45	17.62	19.30	19.06	20.28	18.82	20.05	18.74	18.30	18.48	18.53	19.55	19.91	19.72	19.19
43.65	44.51	42.88	43.67	41.59	43.29	42.12	43.22	44.02	43.98	44.00	42.89	41.98	41.67	43.55
5.40	5.02	5.27	4.83	6.27	5.25	5.21	5.53	4.95	5.07	4.79	5.33	5.80	6.92	4.98
22.04	23.00	21.71	21.81	19.68	21.77	21.79	22.02	22.07	21.63	21.84	20.87	21.05	20.54	21.70
0.34	0.42	0.39	0.40	0.38	0.48	0.41	0.36	0.44	0.35	0.44	0.33	0.39	0.35	0.37
9.34	8.70	9.69	9.56	11.10	9.68	9.71	9.39	9.43	9.66	9.60	10.22	10.16	10.33	9.58

b. Re-crystallized chromite spectrum compositions

Wt%	Spectrum 1	Spectrum 2	Spectrum 3	Spectrum 4	Spectrum 5	Spectrum 6	Spectrum 7	Spectrum 8	Spectrum 9	Spectrum 10
TiO2	0.78	0.82	0.77	0.75	0.69	0.76	0.76	0.69	0.70	0.53
Al2O3	19.78	19.99	20.56	18.87	19.06	19.96	19.73	19.53	19.81	19.91
Cr2O3	45.87	46.37	46.49	44.83	44.63	44.31	44.33	43.55	42.84	43.86
FeO	22.17	21.12	20.09	24.68	24.81	23.44	24.05	25.12	25.11	25.29
MgO	10.87	11.20	11.53	10.37	10.34	11.01	10.68	10.65	11.03	9.94
V2O5	0.52	0.51	0.57	0.51	0.47	0.52	0.45	0.46	0.51	0.47
Cations on basis of 32 oxygens										
Al	5.874	5.920	6.062	5.638	5.691	5.912	5.862	5.806	5.865	5.938
Ti	0.148	0.154	0.145	0.142	0.132	0.144	0.144	0.131	0.132	0.101
Cr	9.136	9.210	9.196	8.985	8.937	8.804	8.834	8.684	8.510	8.777
F33+	0.428	0.308	0.171	0.827	0.860	0.728	0.780	1.001	1.087	0.833
Fe	4.244	4.131	4.033	4.415	4.407	4.207	4.300	4.314	4.207	4.531
Mg	4.084	4.194	4.301	3.919	3.905	4.127	4.014	4.004	4.133	3.751
V	0.087	0.084	0.094	0.085	0.078	0.087	0.075	0.077	0.085	0.079
Mg#	0.490	0.504	0.516	0.470	0.470	0.495	0.483	0.481	0.496	0.453
Al/R3	0.377	0.380	0.389	0.362	0.364	0.379	0.375	0.372	0.376	0.379
Cr/R3	0.586	0.591	0.591	0.576	0.572	0.565	0.566	0.556	0.546	0.561
Ti/R3	0.010	0.010	0.009	0.009	0.008	0.009	0.009	0.008	0.008	0.006
Fe3/R3	0.027	0.020	0.011	0.053	0.055	0.047	0.050	0.064	0.070	0.053
Re-calulated Wt% with Fe2O3										
TiO2	0.78	0.82	0.77	0.74	0.69	0.76	0.76	0.69	0.70	0.53
Al2O3	19.74	19.96	20.54	18.78	18.97	19.87	19.64	19.41	19.68	19.81
Cr2O3	45.76	46.29	46.45	44.61	44.40	44.12	44.12	43.29	42.56	43.64
Fe203	2.25	1.62	0.90	4.31	4.49	3.83	4.09	5.24	5.71	4.35
FeO	20.10	19.63	19.26	20.73	20.70	19.93	20.31	20.33	19.89	21.30
V2O5	0.41	0.39	0.44	0.39	0.36	0.41	0.35	0.36	0.39	0.37
MgO	10.85	11.18	11.52	10.32	10.29	10.97	10.63	10.58	10.96	9.89

c. Chromite rim in contact with sulphide melt spectrum compositions

Wt%	Spectrum 1	Spectrum 2	Spectrum 3	Spectrum 4	Spectrum 5	Spectrum 6	Spectrum 7	Spectrum 8	Spectrum 9	Spectrum 10	Spectrum 11	Spectrum 12	Spectrum 13
TiO2	0.74	0.64	0.77	0.67	0.68	0.76	0.69	0.58	0.66	0.83	0.79	0.88	0.87
Al2O3	22.95	22.95	23.01	22.93	22.73	23.87	23.85	22.68	22.93	22.92	22.99	23.03	22.05
Cr2O3	47.07	46.87	46.73	46.96	46.85	46.41	46.39	47.92	47.76	47.85	47.82	47.63	46.79
FeO	17.25	17.40	17.57	17.47	17.68	16.58	16.62	16.16	16.06	14.93	15.00	14.95	16.76
MgO	11.47	11.47	11.40	11.35	11.49	11.70	11.82	12.09	11.96	12.96	12.84	13.01	13.01
V2O5	0.52	0.68	0.51	0.62	0.57	0.69	0.63	0.56	0.63	0.52	0.55	0.50	0.52
Cations on basis of 32 oxygens													
Al	6.715	6.714	6.734	6.714	6.654	6.948	6.937	6.617	6.689	6.643	6.665	6.668	6.404
Ti	0.138	0.119	0.144	0.126	0.127	0.141	0.128	0.109	0.122	0.153	0.146	0.163	0.162
Cr	9.238	9.199	9.173	9.225	9.200	9.064	9.052	9.376	9.347	9.301	9.302	9.250	9.116
F33+	0.000	0.000	0.000	0.000	0.000	0.000	0.000	0.000	0.000	0.000	0.000	0.000	0.000
Fe	3.580	3.612	3.647	3.630	3.672	3.425	3.430	3.345	3.324	3.069	3.086	3.072	3.453
Mg	4.244	4.245	4.218	4.204	4.254	4.310	4.350	4.461	4.414	4.749	4.711	4.767	4.781
V	0.085	0.111	0.084	0.101	0.093	0.112	0.103	0.092	0.103	0.085	0.090	0.081	0.084
Mg#	0.542	0.540	0.536	0.537	0.537	0.557	0.559	0.571	0.570	0.607	0.604	0.608	0.581
Al/R3	0.417	0.419	0.420	0.418	0.416	0.430	0.430	0.411	0.414	0.413	0.414	0.415	0.408
Cr/R3	0.574	0.574	0.571	0.574	0.576	0.561	0.562	0.582	0.578	0.578	0.577	0.575	0.581
Ti/R3	0.009	0.007	0.009	0.008	0.008	0.009	0.008	0.007	0.008	0.009	0.009	0.010	0.010
Fe3/R3	0.000	0.000	0.000	0.000	0.000	0.000	0.000	0.000	0.000	0.000	0.000	0.000	0.000
Re-calculated Wt% with Fe2O3													
TiO2	0.74	0.64	0.77	0.67	0.68	0.76	0.69	0.58	0.66	0.83	0.79	0.88	0.87
Al2O3	22.95	22.95	23.01	22.93	22.73	23.87	23.85	22.68	22.93	22.92	22.99	23.03	22.05
Cr2O3	47.07	46.87	46.73	46.96	46.85	46.41	46.39	47.92	47.76	47.85	47.82	47.63	46.79
Fe203	0.00	0.00	0.00	0.00	0.00	0.00	0.00	0.00	0.00	0.00	0.00	0.00	0.00
FeO	17.25	17.40	17.57	17.47	17.68	16.58	16.62	16.16	16.06	14.93	15.00	14.95	16.76
V2O5	0.40	0.53	0.40	0.48	0.44	0.53	0.49	0.44	0.49	0.41	0.43	0.39	0.40
MgO	11.47	11.47	11.40	11.35	11.49	11.70	11.82	12.09	11.96	12.96	12.84	13.01	13.01

Chromite rim in contact with sulphide melt spectrum compositions (continued)

Spectrum 14	Spectrum 15	Spectrum 16
0.86	0.90	0.83
22.27	21.76	22.60
47.01	45.73	45.36
15.75	19.52	18.97
13.53	11.62	11.77
0.58	0.46	0.48
6.443	6.383	6.600
0.158	0.169	0.155
9.122	8.998	8.887
0.000	0.000	0.000
3.234	4.061	3.931
4.949	4.313	4.348
0.094	0.076	0.079
0.605	0.515	0.525
0.410	0.410	0.422
0.580	0.579	0.568
0.010	0.011	0.010
0.000	0.000	0.000
0.86	0.90	0.83
22.27	21.76	22.60
47.01	45.73	45.36
0.00	0.00	0.00
15.75	19.52	18.97
0.45	0.36	0.38
13.53	11.62	11.77